

# Isogeometric analysis of $C^1/G^1$ dual mortaring and its application for multi-patch Kirchhoff-Love shell

Di Miao

Advisor: Michael J. Borden

*Department of Civil and Environmental Engineering  
Brigham Young University  
368 CB, Provo, UT 84602, USA*

---

---

## **1. Introduction**

Isogeometric analysis was introduced by Hughes et. al. [49] in 2005, as a novel discretization technology. Since then, it attracted considerable attentions from the academic world and is enjoying explosive growth. The idea behind isogeometric analysis is to use the same basis functions for the geometric modeling and computational analysis. While the main aim of isogeometric analysis is to eliminate the geometric approximation error, it has been observed that, compared to traditional  $C^0$  finite element, higher regularity Non-uniform Rational B-splines (NURBS) provide higher efficiency per degree of freedom [5, 29, 30]. Meanwhile, high regularity basis functions allow us to solve higher order partial differential equations (PDEs), e.g. the biharmonic equation [66, 56, 53], the Kirchhoff-Love shell problem [58, 57, 59] and the Cahn-Hilliard equation [42, 17, 16].

However, the higher dimensional NURBS basis functions are obtained by a tensor product of one-dimensional NURBS basis functions, which imposes limitations on its feasibility for analysis. Considering a scenario that a refinement is applied to a region of interest, however, for the tensor-product domain, it also introduces control points far from that region, which dramatically increases the problem size.

The adaptive finite element technique try to automatically refine a mesh in an optimal fashion so that a desirable discretization error level is achieved

22 with the fewest degrees of freedom. Based on the solution from a coarse  
23 mesh, a *posteriori* error estimator provides a guidance for deciding where  
24 and how to refine a mesh. It can increase the convergence rate, particularly  
25 when singularities are present. However, this promising technique can not  
26 be applied directly to NURBS mesh, as it does not support local refinement.

27 Since high smoothness basis function can be used in Isogeometric analy-  
28 sis, the numerical approximation of high order PDEs can be realized in the  
29 framework of the standard Galerkin formulation. However, without intro-  
30 ducing mesh degenerations, it is impossible to parameterize geometries with  
31 sharp corner or kink by high continuity meshes.

## 32 2. Literature review

33 To circumvent the shortcomings discussed above, various methods have  
34 been proposed. The purpose of this section is to provide an overview of the  
35 popular methods that endow B-spline meshes with multi-patch coupling and  
36 local refinement abilities.

### 37 2.1. Local refinable splines

38 In 1988, Forsey and Bartels [40] introduced the hierarchical B-spline re-  
39 finement algorithm, which can restrict the influence of refinement to the lo-  
40 cality. The algorithm is achieved by a re-representation process that replaces  
41 each basis function by an equivalent linear combination of a set of basis func-  
42 tions defined by nested knot vectors. However, due to the lack of a natural  
43 control grid, the hierarchical B-spline has not been widely recognized in the  
44 CAD society, and a few applications can be found in geometric design. Re-  
45 cently, this technique has been extended to Isogeometric Analysis, by Vuong  
46 *et al.* [87]. Owing to the construction strategy, the resulted hierarchical  
47 basis function are linearly independent and retain the maximal regularity,  
48 which renders the hierarchical B-spline a good candidate for analysis. The  
49 numerical tests demonstrate that the use of the hierarchical B-spline lead to  
50 a superior performance for problems with corner singularity. A subdivision-  
51 based hierarchical B-spline was proposed by Bornemann *et al.* [18], to tackle  
52 the intricate algorithms in the software implementation of hierarchical B-  
53 splines. The subdivision scheme establishes algebraic relations between the  
54 basis functions and their coefficients defined on different refinement level  
55 of the mesh and greatly ease the implementation of hierarchical B-splines.  
56 Consecutively, the truncated basis for hierarchical splines (THB-spline) was

57 introduced by Giannelli *et al.* [41]. THB-splines is created by eliminating  
58 from the coarse hierarchical basis function the contribution corresponding to  
59 the subset of finer basis functions. Besides all the nice properties of hierarchi-  
60 cal B-splines, the THB-splines obtain smaller support and form a partition  
61 of unity, which lead to sparser matrices and lower condition numbers.

62 However, all the above hierarchical B-splines are still under the tensor  
63 product formulism, which restricts hierarchical B-splines to a global rectan-  
64 gular parametric domain. In order to represent complex topologies, subdivi-  
65 sion schemes are widespread in geometry processing and computer graphics.  
66 Among the most popular subdivision schemes are the Catmull-Clark [23],  
67 Doo-Sabin [31] and Loop's [64] scheme. For Isogeometric Analysis, Wei *et*  
68 *al.* [88] introduced truncated hierarchical Catmull-Clark subdivision (THCCS)  
69 that can handle extraordinary nodes involved in complex topologies. THCCS  
70 inherits the surface continuity of Catmull-Clark subdivision, namely  $C^1$   
71 continuity at extraordinary points and  $C^2$  continuity elsewhere. Loop subdivi-  
72 sion surfaces provides similar regularity properties as THCCS and has been  
73 applied to Isogeometric Analysis in [52, 71] to generate triangular meshes.  
74 One of the limitations in the implementation of subdivision meshes is that  
75 the basis function around the extraordinary point is composed of piecewise  
76 polynomial functions with an infinite number of segments, which leads to  
77 insufficient integration by Gauss quadrature rule. To deal with this issue,  
78 various quadrature rules and adaptive strategies have been examined in [67]  
79 for Poisson problem on the disk and in [51] for fourth order PDEs.

80 In 2003, Sederberg *et al.* [79] introduced T-splines, which allows the  
81 existence of T-junctions in the control grid, so that lines of control points  
82 need not traverse the entire control grid. Thus, local refinement can be  
83 realized by introducing T-junctions around interested region. Since the con-  
84 cept of T-splines is a generalization of NURBS technology, it can be used  
85 to merge NURBS surfaces that have different knot-vectors at the intersec-  
86 tion. Therefore, the T-splines are also suitable to address trimmed multi-  
87 patch geometries. Due to the desirable features of T-splines, Bazilevs *et al.*  
88 [4] explored this technology in Isogeometric Analysis, and numerical results  
89 demonstrated its potential for solving structural and fluid problems. By  
90 utilizing the Bézier extraction operator, a finite element data structure for  
91 T-splines [78] was developed to ease the incorporation of T-splines into ex-  
92 isting finite element codes. However, it has been proven [22] that the original  
93 definition of T-splines is not sufficient to ensure the linear independence of  
94 the basis functions. To circumvent this issue, analysis suitable T-splines [63]

95 was developed by applying an additional constraint that no two orthogonal  
96 T-junction extensions are allowed to intersect. Subsequently, the mathematical  
97 properties of analysis suitable T-splines were studied in [62, 91], and it  
98 has been successfully applied to the boundary element method [77]. Mean-  
99 while, an adaptive local h-refinement algorithm with T-splines and a local  
100 refinement of analysis-suitable T-splines were introduced by Döfel *et al.* [37]  
101 and Scott *et al.* [76], respectively. However, for both algorithm, the refined  
102 mesh is not as local as one could hope and this problem might be severe in  
103 3D.

104 *2.2. Multi-patch geometrically continuous functions*

105 One of the advantages of Isogeometric Analysis is that it provides basis  
106 functions with high smoothness, *i.e.* for  $p$ -th order splines, they enjoy up  
107 to  $C^{p-1}$  continuity within a single patch. Thus, it is possible to directly  
108 discretize differential operators of order higher than 2. However, continuity  
109 higher than  $C^0$  for multi-patch discretization imposes significant difficulties.  
110 The conception of geometric continuity is very important in CAD field [73] for  
111 designing smooth multi-patch domain containing extraordinary vertices [72].  
112 In the parametric space, the geometric continuity of order  $s$  ( $G^s$  continuity)  
113 is a weaker continuity constraint as compared to  $C^s$  continuity, while it has  
114 been proved by Giroisser and Peters [43] that  $G^s$  continuity in the parametric  
115 space is equivalent to  $C^s$  continuity of the basis function after the parametric  
116 mapping. Thus, the construction of  $C^s$  isogeometric functions over a  $C^0$   
117 parameterization can be interpreted as geometric continuity  $G^s$  of the graph  
118 parameterization. Bercovier *et al.* [12] has shown that for multi Bézier  
119 patches over an unstructured quadrilateral mesh, as long as the order of  
120 polynomial is high enough, there always exists the minimal determining set  
121 for a  $C^1$  continuity construction. Moreover, the resulting basis functions do  
122 not contain subdivisions around extraordinary vertices.

123 The case of  $G^1$  continuous functions on bilinearly parametrized two-patch  
124 B-spline domains was considered by Kapl *et al.* [56], where the  $C^1$  basis  
125 functions are constructed and analyzed by numerical tests. It is shown that  
126 the space dimensionality heavily depends on the parameterization of two  
127 bilinear patch, and optimal convergence is observed on biharmonic problem.  
128 However, over-constrained  $C^1$  isogeometric spaces that causes sub-optimal  
129 convergence is also observed for certain configurations (*e.g.* two-patch non-  
130 bilinear parameterizations and  $C^{p-1}$  continuity within the patches for  $p$ -th  
131 order spline space). A theoretical analysis of the causing of  $C^1$  locking is

132 provided in [25], where the analysis-suitable  $G^1$  geometry parameterization,  
133 that allows for optimal approximation of  $C^1$  isogeometric spaces, is identified  
134 and testified by numerical examples. The methods in [56] has been extended  
135 to bilinearly parameterized multi-patch domains in [53], where the simple  
136 explicit formulas for spline coefficients of  $C^1$  basis function is derived and  
137 nested  $C^1$  isogeometric spaces are generated. Recently, Kapl *et al.* [55,  
138 54] explored the construction of  $C^2$  isogeometric functions on multi-patch  
139 geometries and utilized the  $C^2$  isogeometric spaces for 6-th order PDE.

140 Although the geometrically continuous functions circumvent the use of  
141 subdivisions for domains with extraordinary vertices, the requirement of  $C^0$   
142 parameterization averts local mesh refinement, and lower continuity is re-  
143 quired to avoid  $C^1$  locking effect. Thus, its implementation can be complex  
144 and it may not be a potential candidate for analysis in more general situa-  
145 tions.

146 *2.3. Variational approach for domain coupling*

147 Unlike geometric design, where high continuity basis functions along the  
148 intersections of neighboring patches are required for the construction of high  
149 quality surface; in analysis, these strong point-wise constraints are unnec-  
150 essarily rigorous, a good approximation of PDEs can be made even if these  
151 constraints are applied in the weak sense. Moreover, the non-conforming  
152 multi-patch coupling is allowed, which maintains the flexibility for the choice  
153 of meshes when multi-patch discretization is needed. Mathematically, the er-  
154 ror estimation of the non-conforming finite element approximation is based on  
155 Strang's lemma [20, 83], which says that for the non-conforming discretized  
156 PDEs, the distance between exact solution to the discrete one is bounded by  
157 the sum of the approximation error and the consistency error. The approx-  
158 imation error measures the failure of discretized finite dimensional space to  
159 capture the exact solution, while the consistency error measures the incon-  
160 sistency between the exact equation and the discretized equation. Various  
161 methods have been developed to eliminate the consistency error and recover  
162 optimal convergence, among them are the mortar method (Lagrange multi-  
163 plier method), stabilized Lagrange multiplier method, the Nitsche's method  
164 and the discontinuous Galerkin (dG) method.

To clearly demonstrate these methods, we consider the following Poisson

problem with homogenous Dirichlet boundary conditions

$$\begin{aligned} -\Delta u &= f, && \text{in } \Omega \\ u &= 0, && \text{on } \partial\Omega \end{aligned} \quad (1)$$

where  $\Omega$  denote a bounded open domain in  $\mathbb{R}^d$ ,  $d = 2$  or  $3$  being the dimension of the problem and its boundary is denoted by  $\partial\Omega$ , in order to simplify the presentation we restrict ourselves to the case of two-dimensional computational domain. The weak form of Equation (1) reads as follow: Find  $u \in H_0^1(\Omega)$  such that

$$a(u, v) = l(v), \quad \forall v \in H_0^1(\Omega), \quad (2)$$

where

$$\begin{aligned} a(u, v) &= \int_{\Omega} \nabla u \cdot \nabla v d\Omega, \\ l(v) &= \int_{\Omega} fv d\Omega. \end{aligned} \quad (3)$$

Using the fact that  $C^0(\Omega) \subset H^1(\Omega)$ , the weak solution can be approximated by considering a finite dimensional continuous function space. Now, we assume that the domain  $\Omega$  is subdivided into  $K$  non-overlapping subdomains or patches  $\Omega_k$  for  $1 \leq k \leq K$ , i.e.

$$\bar{\Omega} = \bigcup_{k=1}^K \bar{\Omega}_k \quad \text{and} \quad \Omega_k \bigcap \Omega_l = \emptyset \quad \forall k \neq l. \quad (4)$$

For simplicity, we only consider the case that the intersection of two patches is either empty or vertex or the entire edge, which rules out the possibility of hanging nodes. We denote the common interface of two neighboring subdomains  $\Gamma_{kl} = \partial\Omega_k \cap \partial\Omega_l$  so that  $\Gamma_{kl} = \emptyset$  if  $\Omega_k$  is not a neighbor of  $\Omega_l$  and define the skeleton  $\mathbf{S} = \bigcup_{k,l \in K, k \neq l} \Gamma_{kl}$  as the union of all interfaces. A representative example of geometry is presented in Figure 1. We can associate each subdomain a bijective geometric mapping as

$$\mathbf{F}_k(\xi_k, \eta_k) : \hat{\Omega}_k \mapsto \Omega_k \in \mathbb{R}^d, \quad (5)$$

where  $\hat{\Omega}_k$  is the parametric domain of  $k^{th}$  patch associated with coordinates  $(\xi_k, \eta_k)$ . For the simplicity and without loss of generality, we assume

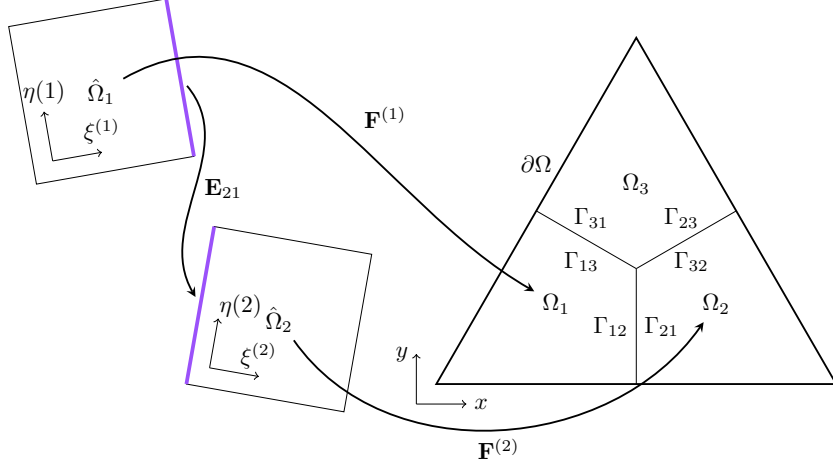


Figure 1: An example of domain decomposition, patches are defined on different parametric domains and are connected via geometric mapping.

<sup>183</sup>  $\hat{\Omega}_k = [0, 1] \times [0, 1]$  for all patches. Due to the difference in the patch pa-  
<sup>184</sup> rameterizations, a physical point on the interface can be mapped to different  
<sup>185</sup> parametric domains with different coordinates. Owing to non-singular pa-  
<sup>186</sup> rameterization, we can establish a bijective transformation from the shared  
<sup>187</sup> edge of  $\hat{\Omega}_k$  to that of  $\hat{\Omega}_l$  by

$$\mathbf{E}_{kl} = (\mathbf{F}_l)^{-1} \circ \mathbf{F}_k. \quad (6)$$

<sup>188</sup>

<sup>189</sup> For each  $\Omega_k$ , we introduce the function space

$$H_*^1(\Omega_k) := \left\{ u \in H^1(\Omega_k) : u = 0 \text{ on } \partial\Omega \cap \partial\Omega_k \right\}, \quad (7)$$

<sup>190</sup> now we can define the broken Sobolev space

$$\mathcal{X} := \left\{ u \in L^2(\Omega) : u|_{\Omega_k} \in H_*^1(\Omega_k) \right\}. \quad (8)$$

<sup>191</sup> Now, the question is how to approximate the weak solution of Equa-  
<sup>192</sup> tion (2) from a finite dimensional subspace of  $\mathcal{X}$ . Since functions in  $\mathcal{X}$  can be  
<sup>193</sup> discontinuous on the skeleton  $\mathbf{S}$ ,  $a(u, u)$  is no longer coercive (or V-elliptic)  
<sup>194</sup> on  $\mathcal{X}$ . As a result, directly using a finite dimensional subspace of  $\mathcal{X}$  to  
<sup>195</sup> discretize Equation (2) will lead to a non-invertible stiffness matrix. Mod-  
<sup>196</sup> ications to the weak form is needed, and we will review some of the most  
<sup>197</sup> popular methods in this section.

198    2.3.1. Lagrange multiplier method

199    The Lagrange multiplier method (or sometimes called mortar method)  
 200    is a domain decomposition technique that allows the coupling of different  
 201    discretization schemes or of non-matching triangulation along interior inter-  
 202    faces. The inter-element continuity condition is enforced weakly by Lagrange  
 203    multipliers. For the Poisson problem, the  $C^0$  continuity constraint is required  
 204    on the intersections, in other words, the jump on the skeleton

$$[u]_{\Gamma_{kl}} := u_k - u_l = 0, \quad \forall \quad \Gamma_{kl} \in \mathbf{S}, \quad (9)$$

205    where  $u_k = u|_{\Omega_k}$ . In order to apply the constraint to the weak form, we  
 206    introduce the potential energy functional:

$$\Pi(v) := \frac{1}{2}a(v, v) - l(v). \quad (10)$$

207    The Equation (2) is equivalent to the minimization problem:

$$\inf_{v \in H_0^1(\Omega)} \Pi(v). \quad (11)$$

208    Then, given a function space  $\mathcal{M}$  defined on the skeleton, a Lagrange multi-  
 209    plier  $\mu \in \mathcal{M}$  is used to add the constraint (9) to the potential energy func-  
 210    tional (10), and the resulted the potential energy functional for the Lagrange  
 211    multiplier method reads

$$\Pi_{LM}(v, \mu) := \Pi(v) + b(\mu, v), \quad (12)$$

212    where

$$b(\mu, v) = \sum_{\Gamma \in \mathbf{S}} \int_{\Gamma} \mu [u]_{\Gamma} d\Gamma. \quad (13)$$

213    The variational formulation of the Lagrange multiplier problem can be de-  
 214    rived from the saddle point problem of the potential energy functional (12)

$$\inf_{v \in X} \sup_{\mu \in \mathcal{M}} \Pi_{LM}(v, \mu), \quad (14)$$

215    as, find  $(u, \lambda) \in \mathcal{X} \times \mathcal{M}$  such that

$$\begin{cases} a(u, v) + b(v, \lambda) = l(v) & \forall v \in \mathcal{X}, \\ b(u, \mu) = 0 & \forall \mu \in \mathcal{M}. \end{cases} \quad (15)$$

216 The solution of the variational formulation is the infimum in  $v$  and the supre-  
 217 mum in  $\mu$ , in other words, it is still a minimization problem in terms of the  
 218 primary variable  $v$  and any function that violate the constraint will be elim-  
 219 inated by the Lagrange multiplier  $\mu$ . This is the reason why it is called the  
 220 saddle point problem. We also denote that the physical meaning of the La-  
 221 grange multiplier  $\mu$  for (12) is the flux of  $v$  over the skeleton. A comprehensive  
 222 study of the mixed problem (15) can be found in [15].

223 In the discretized problem, for a given discrete space  $\mathcal{X}_h$ , the choice of  
 224 the discrete Lagrange multiplier space  $\mathcal{M}_h$  plays a fundamental role for the  
 225 stability of the saddle point problem and the optimality of the discretization  
 226 scheme. To ensure the optimality, the function space for Lagrange multiplier  
 227 should be judiciously chosen so that the consistency error should converges  
 228 at the same rate as that of the approximation error. The feasibility of the  
 229 discrete space pair  $\mathcal{X}_h \times \mathcal{M}_h$  can be measured by the inf-sup test. The inf-sup  
 230 condition is also refered to as the Ladyzhenskaya-Babuska-Brezzi condition  
 231 (or simply LBB). It is a crucial condition to ensure the solvability, stabil-  
 232 ity and optimality of a mixed problem. For the problem (15), the inf-sup  
 233 condition is [15], for  $v \neq 0$  and  $\mu \neq 0$

$$\inf_{\mu \in \mathcal{M}} \sup_{v \in \mathcal{X}} \frac{|b(v, \mu)|}{\|v\|_{\mathcal{X}} \|\mu\|_{\mathcal{M}}} \geq \beta > 0. \quad (16)$$

234 Since the approximation error of problem (15) is given as

$$\|u - u^h\|_{\mathcal{X}} + \|\lambda - \lambda^h\|_{\mathcal{M}} \leq C \left( \inf_{u^h \in \mathcal{X}^h} \|u - u^h\|_{\mathcal{X}} + \inf_{\lambda^h \in \mathcal{M}^h} \|\lambda - \lambda^h\|_{\mathcal{M}} \right), \quad (17)$$

235 where  $C$  is a constant that depends on variables including  $\beta$  but is inde-  
 236 pendent of the mesh size  $h$ . Hence, in a discretized problem, the inf-sup  
 237 condition requires the variable  $\beta$  to be a constant that is independent of the  
 238 mesh size.

239 It is well-known that in order to satisfy the LBB-condition a number of  
 240 possible natural choices for the approximation space pair  $\mathcal{X}_h \times \mathcal{M}_h$  must be  
 241 discarded. In particular, the trace space of slave side, specially convenient  
 242 from the computational point of view, often do not satisfy the LBB-condition  
 243 and can activate pathologies such as spurious oscillations. To remedy this  
 244 problem, the most widely used method in the finite element framework is  
 245 reducing the dimension of Lagrange multiplier space by two (for 2<sup>nd</sup> order  
 246 PDEs). Specifically, the degree of Lagrange multiplier basis functions at both

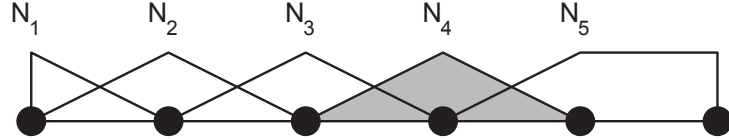


Figure 2: Lagrange multiplier basis functions for the piecewise linear elements, modification on the right end (from Zienkiewicz [92]).

247 ends are reduced by one. This modification has been sucessfully adopted in  
 248 [14, 13, 7, 10, 8, 65, 60, 9]. An example of the modified Lagrange multiplier  
 249 basis functions are illustrated in Figure 2, where the basis function  $N_5$  is  
 250 constant in the right end.

251 In the context of Isogeometric Analysis, the patch coupling problem has  
 252 been firstly studied by Hesch and Betsch [47], where the coupling of La-  
 253 grangian elements and NURBS elements for 3D nonlinear elastic problem  
 254 is validated. To avoid an over constrained linear system, Hesch and Betsch  
 255 used a linear Lagrange multiplier space for higher order NURBS coupling. In  
 256 [21], the choice of the Lagrange multiplier space has been extensively studied,  
 257 it testifies that for equal order pairing, a local degree reduction at extraor-  
 258 dinary vertices is required, and another possibility is reducing the degree of  
 259 Lagrange multiplier space by two compared to the trace space of slave side.  
 260 These choices of Lagrange multiplier spaces are proven to be inf-sup stable  
 261 by various numerical examples. In addition to the constraint on the inter-  
 262 patch displacement, Bouclier *et al.* [19] considered the constraint on the  
 263 traction and claimed that this strategy enables to present a  $C^1$  behavior. In  
 264 the numerical test, smoother displacement fields and smoother stress fields  
 265 are observed.

266 Another drawback of the implementation of mortar methods is that most  
 267 of them introduce Lagrange multipliers as additional variables to enforce  
 268 interface constraints weakly, increasing the problem size. Moreover, different  
 269 physical fields are involved in the weak form, deteriorating the conditioning  
 270 of the global matrix if no appropriate pre-conditioner is applied (detailed  
 271 discussion about preconditioning for saddle point problem can be found in  
 272 [39, 11, 84]).

273    2.3.2. Dual mortar method

274    To circumvent the increase of problem size, we considering the minimiza-  
275    tion problem

$$\inf_{v \in \mathcal{K}} \Pi(v), \quad (18)$$

276    where the function space  $\mathcal{K} = \{v \in \mathcal{X} : b(v, \lambda) = 0, \forall \lambda \in \mathcal{M}\}$ . The mini-  
277    mization problem (18) is indeed equivalent to the saddle point problem (15),  
278    the proof can be found in [15]. Note that, since  $K \subset X$ , the introduce of  
279    Lagrange multiplier indeedly reduces the problem size of (18). Meanwhile,  
280    the symmetric positive definite structure of the resulting stiffness matrix is  
281    preserved. But the construction of the function space  $K$  is not a trivial task.

282    To reduce the cost of constructing the function space  $\mathcal{K}$ , we use the dual  
283    basis functions of the trace space of the slave side as the discrete Lagrange  
284    multiplier space. For a given basis function  $N_i$ , the dual basis function  $\hat{N}_j$  is  
285    defined to satisfy

$$\int_{\Gamma} N_i \hat{N}_j d\Gamma = \delta_{ij} \int_{\Gamma} N_i d\Gamma, \quad (19)$$

286    where  $\delta_{ij}$  is a Kronecker delta function. Of special interest, are biorthogonal  
287    basis functions with compact support, especially

$$\text{supp } \hat{N}_i = \text{supp } N_i. \quad (20)$$

288    Due to the biorthogonality, the discrete bilinear form  $b(v, \mu)$  forms a diagonal  
289    matrix on the slave side, and forms a sparse matrix on the master side.  
290    The function space  $\mathcal{K}$  can be formulated without additional efforts and all  
291    the slave degree of freedom are eliminated in the resulting linear system.  
292    Moreover, owing to the local support property the resulting stiffness matrix  
293    is a symmetric positive definite sparse matrix. Thus, the dual basis functions  
294    are very attractive in the perspective of computational efficiency.

295    Figure 3 shows an example of dual basis functions corresponding to the  
296    basis functions in Figure 2. Again, order reduction is made at the right end.  
297    The dual mortar method was first introduced in [89] for first order finite  
298    element. This method has been extended to higher order degree elements in  
299    [61], to three-dimensional problem in [90] and to contact problem [48, 74].

300    In isogeometric analysis framework, a master-slave type mortar method  
301    has been suggested by Dornisch *et al.* [34], where the weakly applied con-  
302    straint is represented as a master-slave relation and the the slave interface  
303    degrees of freedom (DOF) can be condensed out of the global linear system.

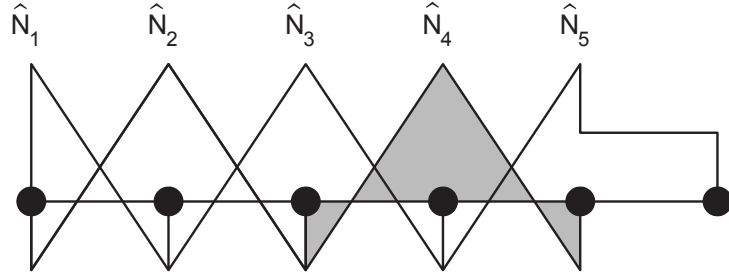


Figure 3: Dual Lagrange multiplier basis functions for the piecewise linear elements, modification on the right end (from Zienkiewicz [92]).

304 Recently, Dornisch *et al.* extended this research to multiple patch coupling in  
 305 [36, 33], where different types of dual basis functions are applied as the basis  
 306 of Lagrange multipliers. The numerical results demonstrate that the approx-  
 307 imate dual basis functions yield accurate result and generate sparse global  
 308 matrix due to the local support. The concept of dual mortar methods is also  
 309 utilized in [80] for contact problem in Isogeometric analysis framework. Coox  
 310 *et al.* [27] proposed an interesting approach to establish the master-slave mor-  
 311 tar method and implemented this approach in [26] to form boundary element  
 312 analysis on complex manifold. In this approach, the master-slave relation are  
 313 formed by knot insertion algorithm and pseudo-inverse.

314 *2.3.3. Perturbed Lagrangian method*

315 Applying constraint by Lagrange multiplier leads to a saddle point prob-  
 316 lem, of which the discrete Lagrange multiplier basis functions cannot be  
 317 chosen independently of that of primal variable and special treatment is  
 318 required on the cross point to ensure the solvability and optimality of the  
 319 discretized system. The stiffness matrix for the discrete problem arising from  
 320 the Lagrangian multiplier method always contains both positive and negative  
 321 eigenvalues, for which iterative methods are known to be less efficient than for  
 322 symmetric positive definite systems. To ensure the invertibility of the stiff-  
 323 ness matrix, a quadratic penalty term is added to the energy functional (12),  
 324 as

$$\Pi_{PLM}(v, \mu) := \Pi_{LM}(v, \mu) - \frac{1}{2\epsilon} \sum_{\Gamma \in S} \int_{\Gamma} \mu^2 d\Gamma, \quad (21)$$

325 where the penalty term is scaled by a parameter  $\epsilon$ . The resulted func-  
 326 tional (21) is referred to as perturbed Lagrangian and the last term is often

327 called stablization term. The resulted variational formulation is stated as

$$\begin{cases} a(u, v) + b(v, \lambda) = l(v) & \forall v \in \mathcal{X}, \\ b(u, \mu) - \frac{1}{\epsilon} \sum_{\Gamma \in \mathbf{S}} \int_{\Gamma} \mu \lambda d\Gamma = 0 & \forall \mu \in \mathcal{M}. \end{cases} \quad (22)$$

328 As  $\epsilon \rightarrow \infty$ , the solution obtained from (22) will converge to the solution ob-  
329 tained by the classical Lagrange multiplier method. For  $0 < \epsilon < \infty$ , any solu-  
330 tion that inconsistent with the constraint will not be fully prohibited, but will  
331 be penalized by the stability term. And the rank of discrete stiffness matrix is  
332 preserved no matter whether the discrete space pair  $\mathcal{X}_h \times \mathcal{M}_h$  fulfills the inf-  
333 sup condition or not. However, for a moderate  $\epsilon$ , the perturbed Lagrangian  
334 method is inconsistent with the classical Lagrange multiplier method, and  
335 the increase of  $\epsilon$  will deteriorate the conditioning of stiffness matrix.

336 The perturbed Lagrangian method has been utilized in [81] for contact  
337 problem and [35, 1] for domain decomposition problem in isogeometric anal-  
338 ysis framework.

### 339 2.3.4. Stabilized Lagrange multiplier method

340 To fully circumvent the inf-sup condition for imposing Dirichlet boundary  
341 by Lagrange multiplier, Barbosa et. al. [3] added a new penalty like term  
342 to the energy functional (12) to enhance the stability. Unlike perturbed  
343 Lagrangian method where the penalty term is inconsistent with the original  
344 problem, the new term proposed by Barbosa maintaining the consistency.  
345 The energy functional of stablized Lagrange multiplier method is given as

$$\Pi_{SLM}(v, \mu) := \Pi_{LM}(v, \mu) - \sum_{\Gamma \in \mathbf{S}} \frac{h}{2\gamma} \int_{\Gamma} (\mu + \left\{ \frac{\partial v}{\partial n} \right\})^2 d\Gamma, \quad (23)$$

346 where  $n$  is the normal vector of the interface,  $h$  is the mesh size on the  
347 intersection,  $\gamma$  is a user defined constant, the average operator

$$\{u\}_{\Gamma_{kl}} := \frac{1}{2} u_k + \frac{1}{2} u_l. \quad (24)$$

348 Since the physical meaning of the Lagrange multiplier is the flux on the  
349 intersection, the stabilization term in (23) is consistent with the original  
350 problem. The resulted variational formulation is stated as

$$\begin{cases} a(u, v) + b(v, \lambda) - \frac{h}{\gamma} \sum_{\Gamma \in \mathbf{S}} \int_{\Gamma} \frac{\partial v}{\partial n} (\lambda + \left\{ \frac{\partial u}{\partial n} \right\}) d\Gamma = l(v) & \forall v \in \mathcal{X}, \\ b(u, \mu) - \frac{h}{\gamma} \sum_{\Gamma \in \mathbf{S}} \int_{\Gamma} \mu (\lambda + \left\{ \frac{\partial u}{\partial n} \right\}) d\Gamma = 0 & \forall \mu \in \mathcal{M}. \end{cases} \quad (25)$$

351 The stabilization parameter  $\gamma$  needs to be carefully chosen. If  $\gamma$  is too large,  
 352 the method degrades to a penalty-type method, with sub-optimal accuracy  
 353 in the asymptotic limit. If  $\gamma$  is too small, the method becomes unstable.  
 354 Recall the trace inequality

$$\|h^{\frac{1}{2}} \frac{\partial u}{\partial n}\|_{\partial\Omega_k}^2 \leq C \|\nabla u\|_{\Omega_k}^2. \quad (26)$$

355 It has been shown [50] that the mixed formulation (25) fulfills the inf-sup  
 356 condition if  $\gamma > 2C$ . The constant  $C$  can be approximated by discretize  
 357 the norms in the inequality (26) and solve the resulting discrete eigenvalue  
 358 problem.

359 It has been demonstrated that there is a close connection with the sta-  
 360 bilized Lagrange multiplier method and Nitsche's method in the context of  
 361 setting the Dirichlet boundary conditions [82] and in the context of domain  
 362 decomposition [46, 45, 50]. Tur et. al. [86] utilized this method to solve  
 363 both small and large deformation contact problems and obtained optimal  
 364 convergence rate for linear elements. To our knowledge, this method has not  
 365 been applied in the isogeometric analysis framework yet.

### 366 2.3.5. Discontinuous Galerkin method

367 Discontinuous Galerkin method (or Nitsche's method) was introduced in  
 368 1971 [69] for handling Dirichlet boundary conditions in the weak sense. Dis-  
 369 continuous Galerkin method resembles a mesh-dependent penalty method.  
 370 Unlike the standard penalty method, which is not consistent unless the  
 371 penalty coefficient goes to infinity, discontinuous Galerkin method is consis-  
 372 tent with the original problem. Moreover, no additional unknown (Lagrange  
 373 multiplier) is needed and no discrete inf-sup condition must be fulfilled, con-  
 374 trarily to mixed methods. Meanwhile, additional term are added into the  
 375 weak form to ensure the ellipticity of the problem.

376 To develop the weak form of discontinuous Galerkin method for homoge-  
 377 neous Poisson problem, we start by multiplying (1) by a test function  $v \in X$   
 378 and integrating by parts, we obtain

$$a(u, v) - \sum_{\Gamma \in \mathbf{S}} \int_{\Gamma} \left\{ \frac{\partial u}{\partial n} \right\} [v] d\Gamma = l(v). \quad (27)$$

379 However, if we consider the right-hand side as a bilinear form, it is not  
 380 coercive. In other words, this problem is not well-posed, since coercive implies

381 the uniqueness of solution. Meanwhile, this bilinear form is not symmetric.  
 382 To recover the symmetry and coercivity of the bilinear form, additional terms  
 383 are needed. To maintain the consistency, the added terms must vanish for  
 384 the true solution. This lead to the following weak form: find  $u \in X$  such  
 385 that

$$a(u, v) - \sum_{\Gamma \in \mathbf{S}} \int_{\Gamma} \left\{ \frac{\partial u}{\partial n} \right\} [v] d\Gamma - \epsilon \sum_{\Gamma \in \mathbf{S}} \int_{\Gamma} \left\{ \frac{\partial v}{\partial n} \right\} [u] d\Gamma + \\ \sum_{\Gamma \in \mathbf{S}} \frac{\gamma}{h} \int_{\Gamma} [u] [v] d\Gamma = l(v) \quad \forall v \in \mathcal{X}. \quad (28)$$

386 Since  $[u] = 0$  on the intersections, the above formulation is consistent with (27).  
 387 Furthermore, and as already stated in [75] the parameter  $\epsilon$  can be set to some  
 388 particular values, namely:

- 389 • For  $\epsilon = +1$ , the resulting method is called the symmetric interior  
 390 penalty Galerkin (SIPG) method. The stiffness matrix of SIPG is sym-  
 391 metric.
- 392 • If  $\epsilon = 0$ , we obtain the incomplete interior penalty Galerkin (IIPG)  
 393 method. It involves only a few terms and is of easiest implementation.
- 394 • If  $\epsilon = -1$ , the resulting method is called the nonsymmetric interior  
 395 penalty Galerkin (NIPG) method. It admits one unique solution and  
 396 converges optimally irrespectively of the value of  $\gamma > 0$ .

397 For  $\epsilon = 0$  and  $\epsilon = +1$ , the bilinear form is coercive if  $\gamma > C$  and  $\gamma > 2C$ ,  
 398 respectively [75]. Similar to the stablized Lagrange multiplier method, the  
 399 discontinuous Galerkin method also requires to solve an eigenvalue problem  
 400 to determine the value of  $\gamma$ .

401 Discontinuous Galerkin method has been widely studied in various as-  
 402 pects, including imposing boundary condition [45], domain decomposition  
 403 [6] and contact problem [24]. In the field of Isogeometric analysis, Discon-  
 404 tinuous Galerkin method has been utilized to imposing Dirichlet boundary  
 405 condition for trimmed spline meshes [38]. The first article discussing discon-  
 406 tinuous Galerkin method based domain decomposition strategy was written  
 407 by Apostolatos *et al.* [2]. Nguyen *et al.* extended it to three-dimensional  
 408 problems in [68]. Guo *et al.* [44] proposed a Nitsche's method for cou-  
 409 pling Kirchhoff-Love NURBS shell patches. Since the governing equation for

Table 1: Property comparison of Lagrange multiplier, dual mortal, perturbed Lagrange multiplier, stablized Lagrange multiplier and discontinuous Galerkin methods.

Methods	well-defined	inf-sup	symmetry	positive definite	size
Lagrange multiplier	depends	depends	yes	no	enlarged
Dual mortar	yes	depends	yes	yes	reduced
Perturbed Lagrange multiplier	yes	depends	yes	no	enlarged
Stabilized Lagrange multiplier	depends	yes	yes	no	enlarged
Discontinuous Galerkin	depends	yes	depends	yes	same

Table 1: Property comparison of Lagrange multiplier, dual mortal, perturbed Lagrange multiplier, stablized Lagrange multiplier and discontinuous Galerkin methods .

410 Kirchhoff-Love shell is 4-th order PDE,  $C^1$  continuity constraint in imposed  
 411 weakly in the method.

412 Although discontinuous Galerkin method does not introduce additional  
 413 DOF and does not need the judicious choice of mutiplier function space,  
 414 the value of the constants in the stablizing term need to be determined.  
 415 Normally, they are determined by solving a eigenvalue problem on the domain  
 416 of the combination of all intersections, which leads to extra computational  
 417 cost. Meanwhile, the additional stablizing terms reduce the sparsity of the  
 418 global linear system. For higher order PDEs, discontinuous Galerkin method  
 419 becomes more complex as higher order derivatives exists in the tractions.

420 A comparison of the variational coupling methods discussed above is  
 421 shown in Table. 1.

### 422 3. Research Objectives

423 My dissertation research focuses on the construction of NURBS basis  
 424 functions among multi-patches that are analysis-suitable for 4<sup>th</sup> order PDEs.  
 425 The coupling constraints are applied weakly by using the dual mortar method.  
 426 The dual basis functions are constructed based on the Bézier probjection  
 427 technology proposed in [85].

### 428 4. Preliminaries

429 This section provides the formulation of univariate basis functions, its  
 430 extention to higher dimensional space, and representations of geometries in  
 431 the context of Isogeometric Analysis. For a detailed explanation we refer to.

432    4.1. Univariate B-spline basis functions

433    A univariate B-spline is piecewise polynomial curve represented as a linear  
 434    combination of B-spline basis functions. Basis functions of  $p^{th}$  order B-spline  
 435    with  $n$  degrees of freedom can be defined by a non-decreasing set of real  
 436    numbers

$$\Xi = \{\xi_1, \xi_2, \dots, \xi_{n+p+1}\}, \quad (29)$$

which is called knot vector. B-splines that are interpolatory at the ends can be achieved by requiring the multiplicity of  $p + 1$  for the first and the last knot. Associated B-spline basis functions are defined using the Cox-de Boor recursion formula:

$$N_{i,0}(\xi) = \begin{cases} 1 & \xi_i \leq \xi \leq \xi_{i+1} \\ 0 & \text{otherwise} \end{cases} \quad (30)$$

$$N_{i,p}(\xi) = \frac{\xi - \xi_i}{\xi_{i+p} - \xi_i} N_{i,p-1}(\xi) + \frac{\xi_{i+p+1} - \xi}{\xi_{i+p+1} - \xi_{i+1}} N_{i+1,p-1}(\xi) \quad (31)$$

437    4.2. Univariate NURBS basis functions

438    The univariate Non-Uniform Rational B-spline (NURBS) can describe  
 439    objects that cannot be represented by polynomial basis, such as circular arcs.  
 440    NURBS are built from B-splines by dividing each B-spline basis functions by  
 441    a weight function

$$W(\xi) = \sum_{j=1}^n w_j N_{j,p} \quad (32)$$

442    and multiplying each B-spline basis functions by the associated weight coeffi-  
 443    cient for the partition of unity. Thus, the NURBS basis functions are defined  
 444    as:

$$R_{i,p}(\xi) = \frac{w_i N_{i,p}}{W(\xi)} \quad (33)$$

445    4.3. Multivariate basis functions

446    For higher dimensional spaces, the B-spline and NURBS basis functions  
 447    can be formed by the Kronecker product of vectors of univariate basis func-  
 448    tions. For a two-dimensional parametric space, given polynomial orders of  
 449     $p_\xi, p_\eta$  and degrees of freedom  $n_\xi, n_\eta$  in  $\xi, \eta$  direction, the bivariate B-spline  
 450    basis functions are defined as:

$$N_{a,\mathbf{p}}(\xi, \eta) = N_{i,p_\xi}(\xi) N_{j,p_\eta}(\eta), \quad (34)$$

<sup>451</sup> where the index  $a$  is defined by the map

$$a = n_\eta i + j. \quad (35)$$

<sup>452</sup> The bivariate NURBS basis functions are defined as

$$R_{a,\mathbf{p}}(\xi, \eta) = \frac{w_a N_{a,\mathbf{p}}}{\sum_{i=1}^n w_i N_{i,\mathbf{p}}}, \quad (36)$$

<sup>453</sup> where  $n = n_\xi \times n_\eta$ . With some abuse of notation, we will drop the dependency  
<sup>454</sup> on the polynomial oder and use  $N_i$  to denote both NURBS basis functions  
<sup>455</sup> and B-spline basis functions in the rest of the paper.

## <sup>456</sup> 5. Weak- $C^1$ coupling for two-patch planar domains

<sup>457</sup> To ground our approach in a practical example, we consider a biharmonic  
<sup>458</sup> problem on a two-patch planar domain, as demonstrated in Figure. 4. The  
<sup>459</sup> domain  $\Omega$  is decomposed to the slave subdomain  $\Omega_s$  (with finer mesh on the  
<sup>460</sup> interface) and the master subdomain  $\Omega_m$  (with coarser mesh on the interface).

In order of focusing on the coupling algorithm itself, we assume the boundaries that neighboring to the common intersection to be homogeneous Neumann boundaries (north and south of  $\Omega_s$  and east and west of  $\Omega_m$ ) and the rest to be homogeneous Dirichlet boundaries (west of  $\Omega_s$  and south of  $\Omega_m$ ), denoted by  $\Gamma_N$  and  $\Gamma_D$  respectively. Then, the strong form of the two-patch biharmonic boundary value problem writes:

$$\begin{aligned} \Delta^2 u &= f, \quad \text{in } \Omega, \\ u &= \frac{\partial u}{\partial \mathbf{n}} = 0, \quad \text{on } \Gamma_D, \\ \Delta u &= \frac{\partial \Delta u}{\partial \mathbf{n}} = 0, \quad \text{on } \Gamma_N. \end{aligned} \quad (37)$$

### <sup>461</sup> 5.1. Continuity constraints

The weak solution of the biharmonic problem (37) is in the space  $H^2(\Omega)$ . Due to the inclusion  $C^1(\Omega) \subset H^2(\Omega)$ , we can use  $C^1$ -continuous functions to approximate the solution. For the two multi-patch domain, constraints

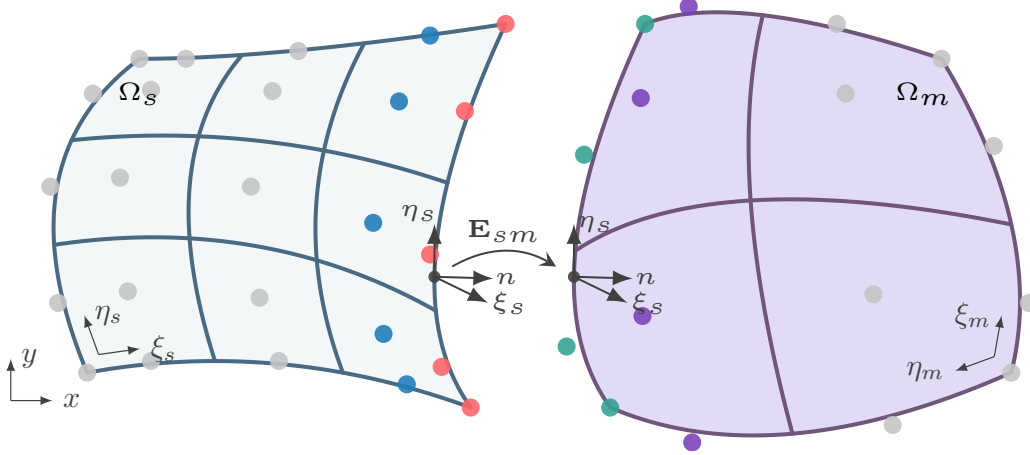


Figure 4: A two-patch planar domain constituted by  $\Omega_m$  and  $\Omega_s$ .

should be added to compromise the discontinuity along the intersection. In general, the following two constraints are requested for  $u$  to be  $C^1$ -continuous

$$[u]_{\Gamma_{sm}} = 0, \quad (38a)$$

$$\left[ \frac{\partial u}{\partial \mathbf{n}} \right]_{\Gamma_{sm}} = 0, \quad \text{with } \mathbf{n} = \mathbf{n}_s = -\mathbf{n}_m \quad (38b)$$

where  $\mathbf{n}_k$  is the outward normal direction of  $\partial\Omega_k$ .

Whereas the constraint (38a) can easily fit into the framework of dual mortar method, the constraint (39) can not be directly imposed. First of all, the existence of dual basis functions of  $\frac{\partial N_i}{\partial \mathbf{n}}|_{\Gamma_{sm}}$  is doubtful. Even if they exist, as they are biorthogonal to the normal derivative of NURBS, their formulation must depend on the parameterization of  $\Gamma_{sm}$ , which violates the virtue of simplicity of dual basis functions. Hence, we need the following result, of which the derivatives are defined in the parametric domain and the dual basis functions can be formulated in an elegant manner.

**Lemma 1.** *Given two differentiable bijective geometric mappings  $\mathbf{F}_s: \hat{\Omega}_s \rightarrow \Omega_s$  and  $\mathbf{F}_m: \hat{\Omega}_m \rightarrow \Omega_m$ , a  $C^0$ -continuous function  $u$  is  $C^1$ -continuous in the physical domain if and only if*

$$\left[ \frac{\partial u}{\partial \xi_s} \right]_{\Gamma_{sm}} = 0 \text{ and } \left[ \frac{\partial u}{\partial \eta_s} \right]_{\Gamma_{sm}} = 0. \quad (39)$$

*Proof.* It suffices to consider two neighboring patches as shown in Figure 4.  $u$  is  $C^0$ -continuous function implies  $\left[ \frac{\partial u}{\partial \eta_s} \right]_{\Gamma_{sm}} = 0$ . For the  $C^1$ -continuity of  $u$ ,

we have the following relation

$$\begin{cases} \frac{\partial u_s}{\partial x} = \frac{\partial u_m}{\partial x} \\ \frac{\partial u_s}{\partial y} = \frac{\partial u_m}{\partial y} \end{cases} \xrightarrow{[\frac{\partial u}{\partial \eta_s}]_{\Gamma_{sm}}=0} \begin{cases} \frac{\partial u_s}{\partial \xi_s} \frac{\partial \xi_s}{\partial x} = \frac{\partial u_m}{\partial \xi_s} \frac{\partial \xi_s}{\partial x} \\ \frac{\partial u_s}{\partial \xi_s} \frac{\partial \xi_s}{\partial y} = \frac{\partial u_m}{\partial \xi_s} \frac{\partial \xi_s}{\partial y} \end{cases} \quad \text{on } \Gamma_{sm} \quad (40)$$

<sup>474</sup> Since the geometric mapping  $\mathbf{F}_s$  is bijective, there exist an inverse mapping  
<sup>475</sup>  $\mathbf{F}_s^{-1}$  and  $\det(\mathbf{F}_s^{-1}) \neq 0$ . Thus,  $[\frac{\partial u}{\partial \xi_s}]_{\Gamma_{sm}} = 0$ . This concludes the proof.  $\square$

The derivatives of  $u_m$  w.r.t.  $\xi_s$  and  $\eta_s$  can be obtained following the chain rule, as

$$\begin{bmatrix} \frac{\partial u_m}{\partial \xi_s} \\ \frac{\partial u_m}{\partial \eta_s} \end{bmatrix} = J(\mathbf{E}_{sm})^T \cdot \begin{bmatrix} \frac{\partial u_m}{\partial \xi_m} \\ \frac{\partial u_m}{\partial \eta_m} \end{bmatrix}, \quad (41)$$

<sup>476</sup> where  $J(\cdot)$  is the Jacobian of the mapping in the argument. The Jacobian of  
<sup>477</sup> the composition mapping  $\mathbf{E}_{sm}$  can be written as

$$J(\mathbf{E}_{sm}) = J((\mathbf{F}_m)^{-1} \circ \mathbf{F}_s) = J((\mathbf{F}_m)^{-1}) \cdot J(\mathbf{F}_s) = J(\mathbf{F}_m)^{-1} \cdot J(\mathbf{F}_s). \quad (42)$$

#### <sup>478</sup> 5.2. Lagrange multiplier formulation and dual mortar formulation

We introduce two Lagrange multiplier spaces:  $M_0$  is devoted to the  $C^0$  constraint (38a) and  $M_1$  is devoted to the  $C^1$  constraint (39). The Lagrange multiplier formulation of the weak problem of (37) reads: find  $u \in X_b$ ,  $\lambda_0 \in M_0$  and  $\lambda_1 \in M_1$  such that:

$$\begin{cases} a_b(u, v) + b_0(\lambda_0, v) + b_1(\lambda_1, v) = l(v), & \forall v \in X_b; \\ b_0(\mu_0, u) = 0, & \forall \mu_0 \in M_0; \\ b_1(\mu_1, u) = 0, & \forall \mu_1 \in M_1; \end{cases} \quad (43)$$

with

$$a_b(u, v) = \int_{\Omega} \Delta u \Delta v d\Omega, \quad (44)$$

$$b_0(\mu, u) = \int_{\Gamma_{sm}} \mu [u]_{\Gamma} d\Gamma, \quad (45)$$

$$b_1(\mu, u) = \int_{\Gamma_{sm}} \mu \left[ \frac{\partial u}{\partial \xi_s} \right]_{\Gamma} d\Gamma. \quad (46)$$

<sup>479</sup> The broken Sobolev space for the biharmonic problem is given as

$$\mathcal{X}_b := \{u \in L^2(\Omega) : u|_{\Omega_k} \in H_*^2(\Omega_k)\}, \quad (47)$$

480 with

$$H_*^2(\Omega_k) := \left\{ u \in H^2(\Omega_k) : u = 0 \text{ and } \frac{\partial u}{\partial \mathbf{n}} = 0 \text{ on } \partial\Gamma_D \cap \partial\Omega_k \right\}. \quad (48)$$

481 By moving the constraints from the problem statement to the definition of the  
482 trial and test function spaces, we obtain the following variational problem:  
483 find  $u \in \mathcal{K}_b$ , such that

$$a_b(u, v) = l(v), \quad \forall v \in \mathcal{K}_b, \quad (49)$$

484 where

$$\mathcal{K}_b := \{u \in \mathcal{X}_b : b_0(u, \mu_0) = 0 \text{ and } b_1(u, \mu_1) = 0 \quad \forall (\mu_0, \mu_1) \in \mathcal{M}_0 \times \mathcal{M}_1\}. \quad (50)$$

485 On one hand, the absence of the Lagrange multipliers  $\lambda_0$  and  $\lambda_1$  reduces the  
486 size of the discretized problem and recovers the symmetric positive definite  
487 structure of the stiffness matrix. As a result, efficient iterative solvers can be  
488 applied for the problem. On the other hand, in the standard formalism,  $\mathcal{M}_0$   
489 and  $\mathcal{M}_1$  are discretized by the trace of one side of the intersection so that  
490 the construction of  $\mathcal{K}_b^h$  requires a factorization of a global constraint matrix,  
491 which is not a trivial task.

492 However, in the following section, we will show that, with the help of dual  
493 basis functions, the discretized function space  $\mathcal{K}_b^h$  can be formulated in an  
494 elegant manner.

### 495 5.3. Finite element approximation

496 Suppose that  $\mathcal{X}_b^h \subset \mathcal{X}_b$ ,  $\mathcal{M}_0^h \subset \mathcal{M}_0$  and  $\mathcal{M}_1^h \subset \mathcal{M}_1$  are finite-dimensional  
497 linear subspaces of the Hilbert spaces  $\mathcal{X}_b$ ,  $\mathcal{M}_0$ , and  $\mathcal{M}_1$ ; we study the finite  
498 element approximation of the abstract problem (43).

**Assumption 1.** All bilinear functionals are bounded; i.e., there exist positive constants  $C_a$ ,  $C_{b_0}$  and  $C_{b_1}$  such that

$$\begin{aligned} |a_b(u, v)| &\leq C_a \|u\|_{H^2} \|v\|_{H^2}, & \forall u, v \in \mathcal{X}_b, \\ |b_0(\mu_0, u)| &\leq C_{b_0} \|\mu_0\|_{L^2} \|u\|_{H^2}, & \forall \mu_0 \in \mathcal{M}_0, u \in \mathcal{X}_b, \\ |b_1(\mu_1, u)| &\leq C_{b_1} \|\mu_1\|_{L^2} \|u\|_{H^2}, & \forall \mu_1 \in \mathcal{M}_1, u \in \mathcal{X}_b. \end{aligned} \quad (51)$$

499 **Assumption 2.** In addition, we assume that the bilinear functional  $a_b(\cdot, \cdot)$   
500 is coercive on  $\mathcal{K}_b$ , i.e.,

$$\exists c_a > 0 \quad s.t. \quad \forall v^h \in \mathcal{K}_b^h, \quad a_b(v^h, v^h) \geq c_a \|v^h\|_{H^2} \quad (52)$$

501     Following standard techniques [20], we now obtain a bound on the error  
 502    between  $u$  and  $u^h$  in term of the best approximation errors, which can be  
 503    considered as Céa's lemma for mixed problems.

504    **Theorem 1.** *Under the above assumptions, there exists a unique solution  
 505     $u^h \in \mathcal{K}_b^h$  satisfies (49). Furthermore,*

$$\|u - u^h\|_{H^2} \leq \left(1 + \frac{C_a}{c_a}\right) \inf_{v^h \in \mathcal{K}_b^h} \|u - v^h\|_{H^2} + \frac{C_b}{c_a} \left( \inf_{\mu_0^h \in \mathcal{M}_0^h} \|\lambda_0 - \mu_0^h\|_{L^2} + \inf_{\mu_1^h \in \mathcal{M}_1^h} \|\lambda_1 - \mu_1^h\|_{L^2} \right), \quad (53)$$

506    where  $C_b = \max(C_{b_0}, C_{b_1})$ .

507    Hence, the error of finite element approximations in broken  $H^2(\Omega)$  norm  
 508    are bounded by the best approximation error of  $v^h \in \mathcal{K}_b^h$  in broken  $H^2(\Omega)$   
 509    norm and  $\mu_0^h \in \mathcal{M}_0^h$ ,  $\mu_1^h \in \mathcal{M}_1^h$  in  $L^2(\Gamma)$  norm. In general, the approximation  
 510    ability of  $p^{th}$  order piecewise polynomial in  $\mathcal{X}_b^h$  is given by

$$\|u - u^h\|_{H^s} \leq Ch^{p+1-s}. \quad (54)$$

511    where  $C$  is a constant that is independent of the mesh size  $h$ . To transform  
 512    approximation estimates in  $\mathcal{K}_b^h$  into standard approximation estimates in  $\mathcal{X}_b^h$ ,  
 513    we need the following assumption:

**Assumption 3.** *Furthermore, we assume that the bilinear functionals  $b_0(\cdot, \cdot)$   
 and  $b_1(\cdot, \cdot)$  are inf-sup stable in the discretized formulation, i.e., there exist  
 positive constants  $\beta_0$  and  $\beta_1$  independent of the mesh size such that*

$$\inf_{\mu_0^h \in \mathcal{M}_0^h} \sup_{u^h \in \mathcal{X}_b^h} \frac{|b_0(\mu_0^h, u)|}{\|u^h\|_{H^2} \|\mu_0^h\|_{L^2}} \geq \beta_0, \quad (55)$$

$$\inf_{\mu_1^h \in \mathcal{M}_1^h} \sup_{u^h \in \mathcal{X}_b^h} \frac{|b_1(\mu_1^h, u)|}{\|u^h\|_{H^2} \|\mu_1^h\|_{L^2}} \geq \beta_1. \quad (56)$$

514    **Theorem 2.** *Under the assumptions, we have that, for any  $u \in \mathcal{K}_b$ ,*

$$\inf_{v^h \in \mathcal{K}_b^h} \|u - v^h\|_{H^2} \leq \left(1 + \frac{C_b}{\beta}\right) \inf_{w^h \in \mathcal{X}_b^h} \|u - w^h\|_{H^2} \quad (57)$$

515    where  $\beta = \min(\beta_0, \beta_1)$ .

516 As can be seen, the optimality of  $u^h \in \mathcal{K}_b^h$  requires the *inf-sup* stability of  
 517 bilinear functional  $b_0$  and  $b_1$ . The analytical study of the *inf-sup* stability is  
 518 beyond the scope of this paper. Instead, we demonstrate the approximation  
 519 ability of  $\mathcal{K}_b^h$  by directly conducting  $H^2$  projection in different numerical  
 520 examples.

521 Meanwhile, the approximation ability of the Lagrange multiplier spaces  
 522  $\mathcal{M}_0^h$  and  $\mathcal{M}_1^h$  also influence the optimality of the finite element approxima-  
 523 tion. Whereas  $u$  is approximated in  $H^2$  space,  $\lambda_0$  and  $\lambda_1$  are approximated in  
 524  $L^2$  space. Hence, the optimality of the finite element approximation requires  
 525 that both  $\mathcal{M}_0^h$  and  $\mathcal{M}_1^h$  are at least  $p - 2$  complete, i.e., functions in  $\mathcal{M}_0^h$  and  
 526  $\mathcal{M}_1^h$  can exactly represent polynomials up to order  $p - 2$ .

#### 527 5.4. Discretization

In order to approximate the solution of the variational problem, we use  
 the NURBS basis functions  $N_i^{(s)}$   $i \in I_s$  and  $N_j^{(m)}$   $j \in I_m$  to discretize coupled  
 patches  $\Omega_s$  and  $\Omega_m$ , respectively. An appropriate offset has been made so  
 that there is no overlapping between index sets  $I_s$  and  $I_m$  (given  $n_s$  basis  
 functions in  $\Omega_s$ , we can assume the starting index in the index set  $I_m$  is  
 $n_s + 1$ ). The discretized geometrical mappings are represented by

$$\mathbf{F}_s = \sum_{i \in I_s} \mathbf{P}_i^s N_i^s, \quad (58)$$

$$\mathbf{F}_m = \sum_{i \in I_m} \mathbf{P}_i^m N_i^m, \quad (59)$$

528 where the control points  $\mathbf{P}_i^s, \mathbf{P}_i^m \in \mathbb{R}^2$ . The same basis functions are also  
 529 used to discretize the test function  $u$  in broken Sobolev space  $\mathcal{X}_b$ , as

$$u^h = \sum_{i \in I_s + I_m} U_i N_i, \quad (60)$$

with

$$N_i = \begin{cases} N_i^s, & i \in I_s; \\ N_i^m, & i \in I_m. \end{cases} \quad (61)$$

530 As compared to the standard formalism that utilizes the trace of the slave  
 531 patch on the intersection as the discretization of Lagrange multipliers, in this  
 532 research, we construct Lagrange multipliers by using Bézier dual basis. We  
 533 first classify NURBS basis functions into five different kinds, as shown in  
 534 Figure. 4, namely:

- 535 1. The basis functions  $N_i^{(s)}$  such that  $\text{supp}(N_i^{(s)}) \cap \Gamma_{sm} = \emptyset$  and  $\text{supp}(\frac{\partial N_i^{(s)}}{\partial \xi_s}) \cap \Gamma_{sm} \neq \emptyset$ , whose indices are in the index set  $I_i$ . (denoted by blue dots)
- 536 2. The basis functions  $N_i^{(s)}$  such that  $\text{supp}(N_i^{(s)}) \cap \Gamma_{sm} \neq \emptyset$ , whose indices are in the index set  $I_{ii}$ . (denoted by red dots)
- 537 3. The basis functions  $N_i^{(m)}$  such that  $\text{supp}(N_i^{(m)}) \cap \Gamma_{sm} = \emptyset$  and  $\text{supp}(\frac{\partial N_i^{(m)}}{\partial \xi_s}) \cap \Gamma_{sm} \neq \emptyset$ , whose indices are in the index set  $I_{iii}$ . (denoted by green dots)
- 538 4. The basis functions  $N_i^{(m)}$  such that  $\text{supp}(N_i^{(m)}) \cap \Gamma_{sm} \neq \emptyset$ , whose indices are in the index set  $I_{iv}$ . (denoted by purple dots)
- 539 5. All basis functions neither the supports of themselves nor the supports of their first order derivatives in  $\xi_s$  direction intersect with  $\Gamma_{sm}$ , whose indices are in the index set  $I_v$ . (denoted by grey dots)

540  
541  
542  
543  
544  
545 For the basis functions of the second kind, their restrictions on the intersection  $\Gamma_{sm}$  are one dimensional NURBS basis functions  $N_{i,p_\eta}^{(s)} i \in \{1, 2, \dots, n_\eta^s\}$  that are used to discretize the tensor-product domain  $\Omega_s$  in  $\eta$  direction. In order to obtain an Identity matrix on the slave side of the discretized bilinear form  $b_0$ , the associated dual basis functions of  $N_{i,p_\eta}^{(s)}$  are used to discretize the Lagrange multiplier space  $\mathcal{M}_0$ , as

$$\lambda_0^h = \sum_{i=1}^{n_\eta^s} \Lambda_i^0 \hat{N}_{i,p_\eta}^{(s)}. \quad (62)$$

552 For the basis functions of the first kind, the restrictions of their first order  
553 derivatives on the intersection  $\Gamma_{sm}$  can be written as  $c N_{i,p_\eta}^{(s)} i \in \{1, 2, \dots, n_\eta^s\}$ ,  
554 with  $c = N_{n_\xi^s-1,p_\xi}^{(s)}(1)$ . Hence, the Lagrange multiplier space  $\mathcal{M}_1$  can be  
555 discretized by

$$\lambda_1^h = \sum_{i=1}^{n_\eta^s} \Lambda_i^1 \tilde{N}_i, \quad \text{with } \tilde{N}_i = \frac{1}{c} N_{i,p_\eta}^{(s)}. \quad (63)$$

556 We denote the basis functions in  $\mathcal{M}_0^h$  and  $\mathcal{M}_1^h$  as the dual basis functions of  
557 the second and the first kinds of NURBS basis functions, respectively.

558 By substituting these NURBS approximations into the Lagrange multi-  
559 plier formulation (43), we obtain the following linear system:

$$\begin{bmatrix} \mathbf{K} & \mathbf{B}^T \\ \mathbf{B} & \mathbf{0} \end{bmatrix} \begin{bmatrix} \mathbf{U} \\ \boldsymbol{\Lambda}_0 \\ \boldsymbol{\Lambda}_1 \end{bmatrix} = \begin{bmatrix} \mathbf{F} \\ \mathbf{0} \end{bmatrix}, \quad (64)$$

560 where  $\mathbf{K}$  and  $\mathbf{F}$  are the stiffness matrix and the load vector for the uncoupled  
 561 problem, respectively.  $\mathbf{B}$  is the constraint matrix discretized from the bilinear  
 562 forms  $b_0$  and  $b_1$ . In order to construct the finite element space  $\mathcal{K}_b^h$ , we need to  
 563 solve the constraint matrix  $\mathbf{B}$ 's null space  $\mathbf{C} = \ker(\mathbf{B})$ . Since the structure of  
 564 the constraint matrix  $\mathbf{B}$  depends on the index sets  $I_s$  and  $I_m$  and the ordering  
 565 of Lagrange multiplier basis functions, without adding any constraints on the  
 566 indices, we introduce two permutation matrices  $\mathbf{P}_c$  and  $\mathbf{P}_r$  (this step is not  
 567 necessary from the implementation point of view, but is very convenient  
 568 for the demonstration, especially for multi-patch problem). We define the  
 569 column permutation matrix  $\mathbf{P}_c$  as

$$\begin{bmatrix} \mathbf{I}_i \\ \mathbf{I}_{ii} \\ \mathbf{I}_{iii} \\ \mathbf{I}_{iv} \\ \mathbf{I}_v \end{bmatrix} = \mathbf{P}_c \begin{bmatrix} \mathbf{I}_s \\ \mathbf{I}_m \end{bmatrix}, \quad (65)$$

570 where  $\mathbf{I}_i$  is the vector form of the index set  $I_i$ . For an appropriate row  
 571 permutation matrix  $\mathbf{P}_r$ , the modified constraint matrix can be written in a  
 572 partitioned form as

$$\mathbf{B}_p = \mathbf{P}_r \mathbf{B} \mathbf{P}_c^T = \begin{bmatrix} \mathbf{B}_1^1 & \mathbf{B}_1^2 & \mathbf{B}_1^3 & \mathbf{B}_1^4 & \mathbf{0} \\ \mathbf{0} & \mathbf{B}_2^2 & \mathbf{B}_2^3 & \mathbf{0} & \mathbf{0} \end{bmatrix}, \quad (66)$$

573 where  $\mathbf{B}_i^j$  corresponds to the contribution of the inner product of the basis  
 574 functions of the  $j^{th}$  kind with the dual basis functions of the  $i^{th}$  kind.  $\mathbf{P}_r$   
 575 can be defined as a row permutation matrix such that the resulted block  
 576 sub-matrices  $\mathbf{B}_1^1$  and  $\mathbf{B}_2^2$  are both identity matrices. Under a rank-preserving  
 577 transformation  $\mathbf{T}$ , we can eliminate the block sub-matrix  $\mathbf{B}_1^2$ , as

$$\mathbf{T}\mathbf{B}_p = \begin{bmatrix} & \mathbf{I} & \begin{array}{|c|c|c|c|} \hline & \mathbf{B}_1^3 - \mathbf{B}_1^2 \mathbf{B}_2^3 & \mathbf{B}_1^4 & \mathbf{0} \\ \hline & \mathbf{B}_2^3 & \mathbf{0} & \mathbf{0} \\ \hline \end{array} \end{bmatrix}. \quad (67)$$

578 We may now take

$$\mathbf{C}_p := \ker(\mathbf{B}_p) = \begin{bmatrix} \mathbf{B}_1^2 \mathbf{B}_2^3 - \mathbf{B}_1^3 & -\mathbf{B}_1^4 & \mathbf{0} \\ -\mathbf{B}_2^3 & \mathbf{0} & \mathbf{0} \\ \hline & \mathbf{I} & \end{bmatrix}. \quad (68)$$

<sup>579</sup> Hence, the null space of  $\mathbf{B}$  can be taken as

$$\mathbf{C} = \mathbf{P}_c^T \mathbf{C}_p. \quad (69)$$

<sup>580</sup> Now we can discretize functions in  $\mathcal{K}_b^h$  as

$$u^h = \mathbf{N}^T \mathbf{U}, \quad \text{with } \mathbf{U} = \mathbf{C} \tilde{\mathbf{U}}, \quad (70)$$

<sup>581</sup> where  $\mathbf{N}$  is the vector form of basis functions of  $\mathcal{X}_b^h$ , and  $\tilde{\mathbf{U}}$  is the control  
<sup>582</sup> point vector. By substituting the above discretization in the weak form (50),  
<sup>583</sup> we obtain the following linear system to be solved:

$$\mathbf{C}^T \mathbf{K} \mathbf{C} \tilde{\mathbf{U}} = \mathbf{C}^T \mathbf{F}. \quad (71)$$

<sup>584</sup> Because of the biorthogonality of the NURBS basis functions and their dual  
<sup>585</sup> basis functions, the constrained solution spcae  $\mathcal{K}_b^h$  can be constructed very  
<sup>586</sup> efficiently, leading to a sparse, symmetric positive definite formulation.

## <sup>587</sup> 6. Weak- $C^1$ coupling for multi-patch planar domains

<sup>588</sup> To generate complex geometries, we need to decompose domain to mul-  
<sup>589</sup> tiple patches. Unfortunately, we cannot apply directly the results of two-  
<sup>590</sup> patch coupling to this more general mortar situation. The main issue is  
<sup>591</sup> the so-called cross points. For a multi-patch decomposition, at least three  
<sup>592</sup> subdomains meet at an interior crosspoint and several interfaces can share  
<sup>593</sup> this cross point as a common endpoint (Figure. 5). If we use the discretized  
<sup>594</sup> Lagrange multipliers proposed in the previous section, owing to the presence  
<sup>595</sup> of cross points, some of the control points will serve as both slave points  
<sup>596</sup> (indices in  $I_1$  and  $I_2$ ) and master points (indices in  $I_3$  and  $I_4$ ). Hence, there  
<sup>597</sup> is no permutation matrices such that the constraint matrix  $\mathbf{B}$  can be mod-  
<sup>598</sup> ified to the form as equation (67), of which the null space can be found in  
<sup>599</sup> a trivial way. Even more, although the constraint matrices defined on each  
<sup>600</sup> interfaces are full row rank, the assembled constraint matrix  $\mathbf{B}$  may not be  
<sup>601</sup> full row rank in most cases, which renders the linear system (64) to be rank  
<sup>602</sup> deficient. As a result, either modifications to the Lagrange multipliers or to  
<sup>603</sup> the method itself is required so that the proposed method can be generalized  
<sup>604</sup> to a setting where a domain can be decomposed to an arbitrary number of  
<sup>605</sup> patches. Before we start this section, we would like to introduce the sixth  
<sup>606</sup> kind of NURBS basis function that associated with the cross point  $v$ , as

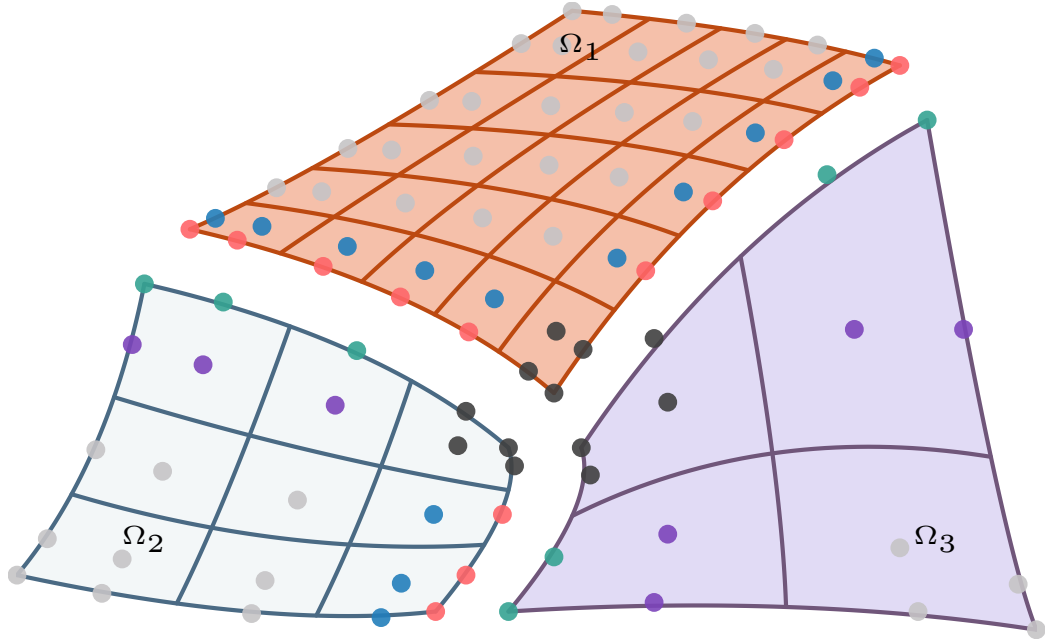


Figure 5: A three-patch planar domain constituted by  $\Omega_1$ ,  $\Omega_2$  and  $\Omega_3$ .

- 607     6. The basis function  $N_i$  such that  $\text{supp}(N_i) \cap v \neq 0$ , or  $\text{supp}(\frac{\partial N_i}{\partial \xi}) \cap v \neq$   
608       0, or  $\text{supp}(\frac{\partial N_i}{\partial \eta}) \cap v \neq 0$  or  $\text{supp}(\frac{\partial^2 N_i}{\partial \xi \partial \eta}) \cap v \neq 0$ , whose indices are in the  
609       index set  $I_{vi}$ . (denoted by black dots in Figure. 5)
- 610     The rest five kinds of NURBS basis function remain the same except their  
611       intersection with the sixth kind are excluded, that is

$$I_k = I_k - I_{vi} \bigcap I_k, \quad k \in \{i, ii, \dots, v\}. \quad (72)$$

- 612     The basis functions in  $\mathcal{M}_0^h$  and  $\mathcal{M}_1^h$  can be classified as the dual basis func-  
613       tions of the NURBS basis function of the 1<sup>st</sup>, 2<sup>nd</sup> and 6<sup>th</sup> kind, respectively.  
614     The domains on the two sides of each interface can still be considered as slave  
615       and master based on the same rule as for the two-patch coupling case.

### 616     6.1. Cross point modification

617     Since using the discretization of Lagrange multipliers proposed for two-  
618       patch coupling case directly results in over-constrained constraint matrix  $\mathbf{B}$   
619       for the control points round the crosspoints, we can remedy this issue by re-  
620       ducing the dimension of the Lagrange multiplier spaces. Roughly speaking,

621 we have to remove the two degrees of freedom of the Lagrange multiplier  
 622 spaces associated with each cross point so that the resulted Lagrange multi-  
 623 plier spaces on each interface should have the same dimension as  $\mathcal{X}_b^h|_{\Omega_s} \cap H_0^2(\Gamma_{sm})$ .

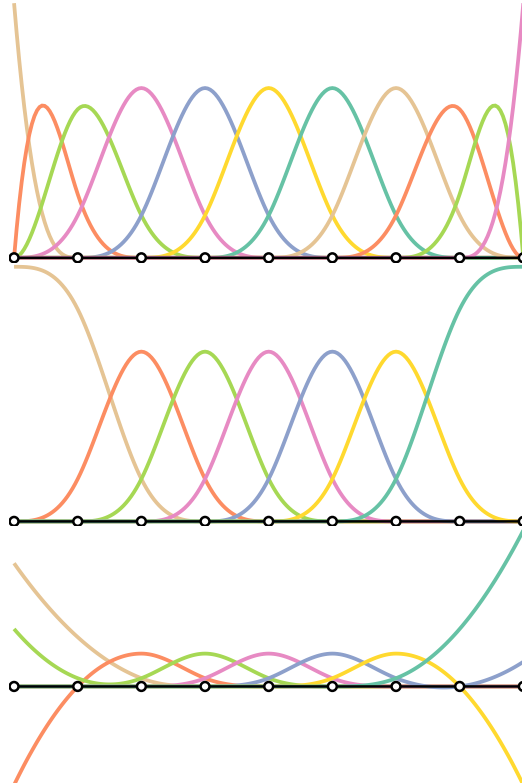


Figure 6: Quadratic basis functions and their cross point modifications. Top: original quadratic basis functions. Middle: coarsened basis functions. Bottom: degree reduced basis functions

624 This can be achieved by two ways: we can either coarse the mesh for the  
 625 Lagrange multiplier in the neighborhood of the cross point, or reduce their  
 626 polynomial degree in the neighborhood of the cross point. An example for  
 627 quadratic 1-D B-spline basis functions is shown in Figure. 6. The coarsened  
 628 basis functions are achieved by replacing the first three and last three basis  
 629 functions by their summations, while we can construct degree reduced basis  
 630 functions by reduce the polynomial degree of the first and last two elements  
 631 by one while retaining the inter-element continuity.

632 Although the degree reduction is not a trivial task for dual basis, the  
 633 summation trick can be applied to coarse dual basis functions. After the

634 coarsen procedure, the dual basis functions associated with the basis func-  
 635 tions of 6<sup>th</sup> kind are all eliminated so that no inter-dependencies will happen  
 636 in the neighborhood of the cross point. We can define a column permutation  
 637 matrix

$$\begin{bmatrix} \mathbf{I}_i \\ \mathbf{I}_{ii} \\ \mathbf{I}_{iii} \\ \mathbf{I}_{iv} \\ \mathbf{I}_{vi} \\ \mathbf{I}_v \end{bmatrix} = \tilde{\mathbf{P}}_c \begin{bmatrix} \mathbf{I}_1 \\ \mathbf{I}_2 \\ \mathbf{I}_3 \end{bmatrix}. \quad (73)$$

638 With a suitable row permutation matrix  $\tilde{\mathbf{P}}_r$ , the constraint matrix  $\mathbf{B}$  can be  
 639 modified as

$$\tilde{\mathbf{B}}_p := \tilde{\mathbf{P}}_r \mathbf{B} \tilde{\mathbf{P}}_c^T = \begin{bmatrix} \mathbf{B}_1^1 & \mathbf{B}_1^2 & \mathbf{B}_1^3 & \mathbf{B}_1^4 & \mathbf{B}_1^6 & \mathbf{0} \\ \mathbf{0} & \mathbf{B}_2^2 & \mathbf{B}_2^3 & \mathbf{0} & \mathbf{B}_2^6 & \mathbf{0} \end{bmatrix}, \quad (74)$$

640 with  $\mathbf{B}_1^1$  and  $\mathbf{B}_2^2$  be identity matrices. Hence, its null space can be found as

$$\tilde{\mathbf{C}}_p := \ker(\tilde{\mathbf{B}}_p) = \begin{bmatrix} \mathbf{B}_1^2 \mathbf{B}_2^3 - \mathbf{B}_1^3 & -\mathbf{B}_1^4 & -\mathbf{B}_1^6 & \mathbf{0} \\ -\mathbf{B}_2^3 & \mathbf{0} & -\mathbf{B}_2^6 & \mathbf{0} \\ \vdots & & \vdots & \\ \mathbf{I} & & & \end{bmatrix}. \quad (75)$$

641 Although the boundary modification by coarsening eliminates the inter-dependency  
 642 in the neighborhood of cross points, numerical tests demonstrate sub-optimality.

### 6.2. Explicitly solve the null space

644 Instead of modifying the Lagrange multipliers, we can solve the null space  
 645 of the over-constrained constraint matrix  $\mathbf{B}$  directly. Seveal matrix factoriza-  
 646 tion methods can be used to solve the null space, including LU, QR, SVD. For  
 647 example, a rank-revealing QR factorization over a rank-deficiency constraint  
 648 matrix  $\mathbf{B}$  yields

$$\mathbf{B}\mathbf{P} = \mathbf{Q} \begin{bmatrix} \mathbf{R}_1 & \mathbf{R}_2 \\ \mathbf{0} & \mathbf{0} \end{bmatrix} \quad (76)$$

649 where  $\mathbf{P}$  is a permutation matrix,  $\mathbf{Q}$  is an unitary matrix,  $\mathbf{R}_1$  is a upper  
 650 triangular matrix and  $\mathbf{R}_2$  is a rectangular matrix. The null space can be  
 651 taken as

$$\ker(\mathbf{B}) = \mathbf{P} \begin{bmatrix} -\mathbf{R}_1^{-1} \mathbf{R}_2 \\ \mathbf{I} \end{bmatrix}. \quad (77)$$

652 However, this requires a factorization of the entire constraint matrix  $\mathbf{B}$  and  
 653 we fail to utilize the advantage of the Bézier dual basis. Even more, the  
 654 sparsity of the constrained stiffness matrix might be impacted as the inverse  
 655 of  $\mathbf{R}_1$  is a dense matrix. This type of global factorization has been utilized  
 656 for patch coupling problem in [27, 28, 32].

657 Instead of solving the null space directly, we will localize the constraint  
 658 to each cross point and solve the null space of a localized linear system. For  
 659 the constraint matrix  $\mathbf{B}$  constructed by the Lagrange multipliers without  
 660 modification, we assume there exist a row permutation matrix  $\hat{\mathbf{P}}_r$  such that

$$\hat{\mathbf{B}}_p := \hat{\mathbf{P}}_r \mathbf{B} \tilde{\mathbf{P}}_c^T = \begin{bmatrix} \mathbf{B}_1 \\ \mathbf{B}_2 \end{bmatrix} = \begin{bmatrix} \mathbf{B}_6^1 & \mathbf{B}_6^2 & \mathbf{B}_6^3 & \mathbf{B}_6^4 & \mathbf{B}_6^6 & \mathbf{0} \\ \mathbf{B}_1^1 & \mathbf{B}_1^2 & \mathbf{B}_1^3 & \mathbf{B}_1^4 & \mathbf{B}_1^6 & \mathbf{0} \\ \mathbf{0} & \mathbf{B}_2^2 & \mathbf{B}_2^3 & \mathbf{0} & \mathbf{B}_2^6 & \mathbf{0} \end{bmatrix}, \quad (78)$$

661 with  $\mathbf{B}_1^1$  and  $\mathbf{B}_2^2$  be identity matrices.  $\mathbf{B}_1$  consists of constraints relevant to  
 662 cross point while  $\mathbf{B}_2$  consists of constraints relevant to intersections.

663 The null space of  $\mathbf{B}_2$  can be found as

$$\mathbf{C}_2 := \ker(\mathbf{B}_2) = \begin{bmatrix} \mathbf{B}_1^2 \mathbf{B}_2^3 - \mathbf{B}_1^3 & -\mathbf{B}_1^4 & -\mathbf{B}_1^6 & \mathbf{0} \\ -\mathbf{B}_2^3 & \mathbf{0} & -\mathbf{B}_2^6 & \mathbf{0} \\ \mathbf{I} \end{bmatrix}. \quad (79)$$

Due to the inclusion  $\hat{\mathbf{C}}_p := \ker(\hat{\mathbf{B}}_p) \subset \ker(\mathbf{B}_2)$ , we can construct  $\hat{\mathbf{C}}_p$  by

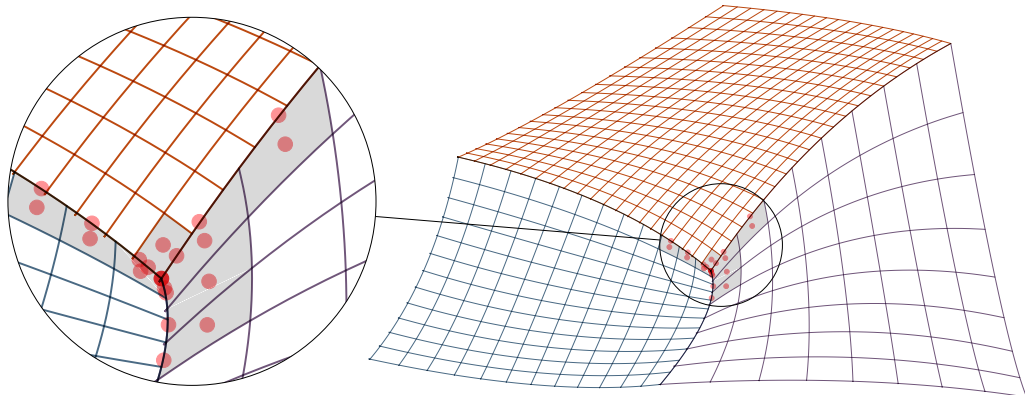


Figure 7: Control points (red) involved in crosspoint constraints ( $\mathbf{B}_1$ ).

solving  $\ker(\mathbf{B}_1 \mathbf{C}_2)$ . Since dual basis functions have compact support,  $\mathbf{B}_1$  and

$\mathbf{C}_2$  are all sparse matrices (control points involved in  $\mathbf{B}_1$  are demonstrated in Figure. 7). We can split the columns of  $\mathbf{C}_2$  into two matrices, as

$$\begin{aligned}\mathbf{C}_2^1 &:= \{v \in \mathbf{C}_2 : \mathbf{B}_1 v \neq 0\}, \\ \mathbf{C}_2^2 &:= \{v \in \mathbf{C}_2 : \mathbf{B}_1 v = 0\}.\end{aligned}\quad (80)$$

Such a split can be defined a priori, based on the discretization of each patch. A demonstration of the split is given in Figure. 8. Note that  $\mathbf{C}_2^2 \subset \hat{\mathbf{C}}_p$ ,  $\hat{\mathbf{C}}_p$  can be written as

$$\hat{\mathbf{C}}_p = [\mathbf{C}_2^1 \ker(\bar{\mathbf{B}}_p) \quad \mathbf{C}_2^2], \text{ with } \bar{\mathbf{B}}_p = \mathbf{B}_1 \mathbf{C}_2^1. \quad (81)$$

Compared with the constraint matrix  $\mathbf{B}$  whose size increases as we refine

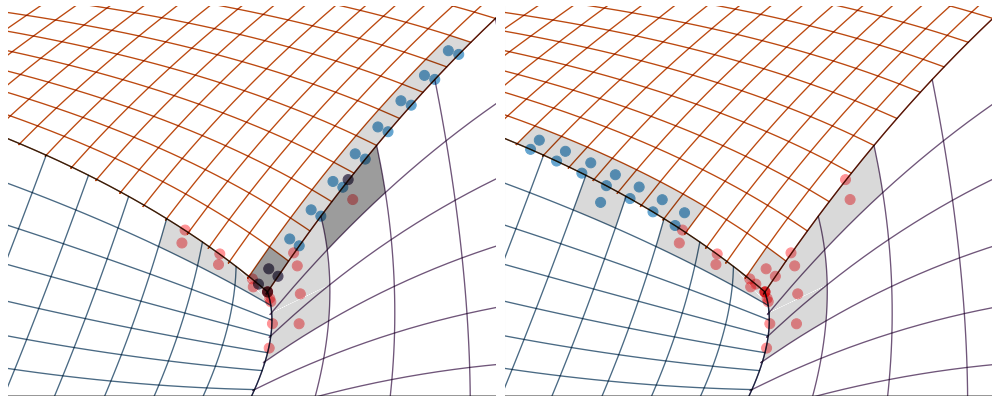


Figure 8: Control points of basis functions (blue) defined by columns of  $\mathbf{C}_2$ . Left: Basis classified to  $\mathbf{C}_2^1$ ; Right: Basis classified to  $\mathbf{C}_2^2$

the mesh, the row size of  $\bar{\mathbf{B}}_p$  is fixed and its column size is fixed after certain refinement. A comparison of the size of matrix  $\mathbf{B}$  and matrix  $\bar{\mathbf{B}}_p$  as a function of the degrees of freedom is given in Figure. 9 for the three-patch coupling in Figure. 5 with 2<sup>nd</sup> order B-spline basis functions. As can be seen, the size of  $\mathbf{B}$  grows rapidly as the mesh being refined. The computational cost of directly solving its kernel will be very expensive. However, owing to the compact support of dual basis function, we can transfer a global, size-varying problem (factorization on  $\mathbf{B}$ ) to a local, size-fixed problem (factorization on  $\bar{\mathbf{B}}_p$ ), and the problem size is very small ( $12 \times 24$  for this case).

A graphical comparison of the sparsity patterns among standard Lagrange multiplier with global factorization, Bézier dual basis with global factorization and Bézier dual basis with local factorization is given in Figure. 10.

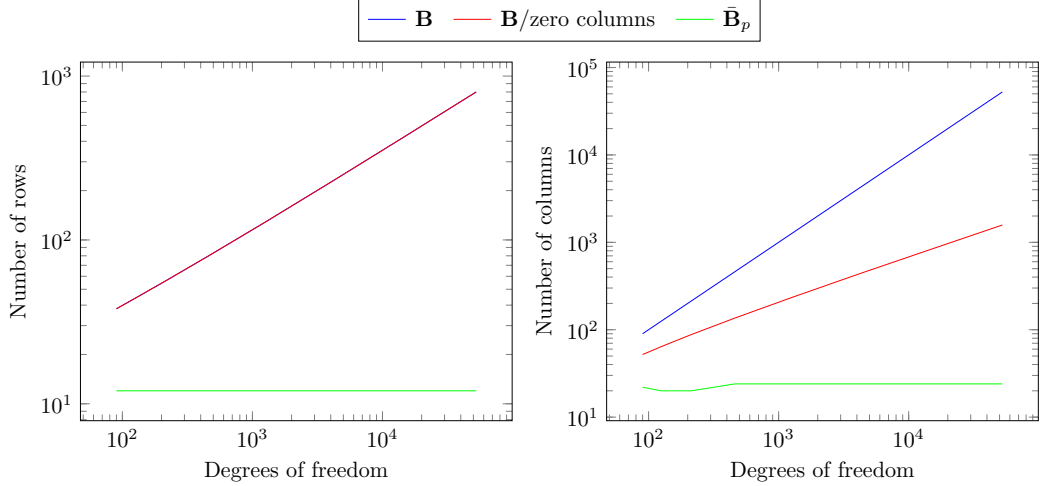


Figure 9: The change of matrix size of  $\mathbf{B}$ ,  $\mathbf{B}$  with zero columns being removed, and  $\bar{\mathbf{B}}_p$ , as a function of the degrees of freedom. The constraint matrix  $\mathbf{B}$  is formulated for the three-patch coupling in Figure. 5 with 2<sup>nd</sup> order B-spline basis functions.

680 As expected, the standard method yields the lowest sparsity, while Bézier  
 681 dual basis with local factorization yields the highest sparsity (40% sparser).  
 682 Meanwhile, the Bézier dual basis does not significantly improve the sparsity  
 683 if a global factorization is applied to construct  $\mathcal{K}_b^h$ . Moreover, a global fac-  
 684 torization yeilds entries with very small absolute values ( $\leq 10^{-14}$ ), especially  
 685 for the constraint matrix formed by Bézier dual basis, while all entries are  
 686 away from zero for the local factorization.

## 687 7. Numerical results

688 All our numerical results are obtained via an in-house C++ code.

### 689 7.1. A numerical study of the completeness of Bézier dual basis

690 We consider the completeness of Bézier dual basis on the one dimensional  
 691 domain,  $\Omega = (0, 1)$ . The domain  $\Omega$  is uniformly partitioned into two elements,  
 692 since the Bézier dual basis is equivalent to the global dual basis on one  
 693 element domain. In the numerical test, we find the  $L^2$  approximation of  $n^{th}$   
 694 order Legendre polynomial in the Bézier dual space, as Legendre polynomials  
 695 are orthogonal to each other.

696 The test results are disappointed, the Bézier dual basis of arbitrary order  
 697 is only complete for zeroth order polynomial i.e., only the error of the  $L^2$

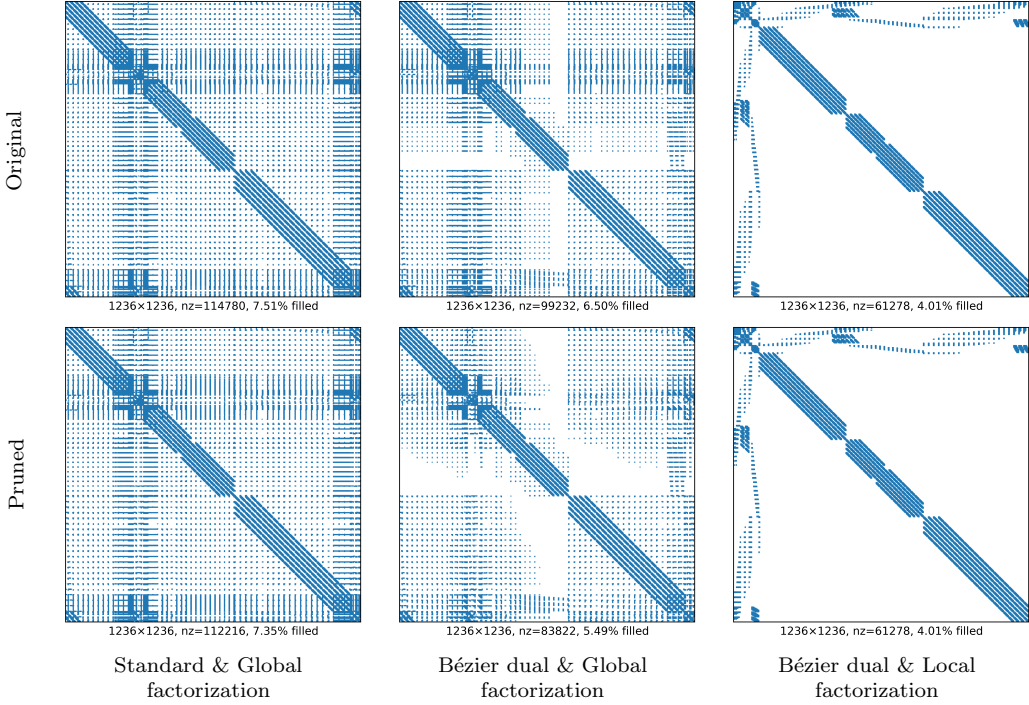


Figure 10: Sparsity patterns of constrained stiffness matrices. Left: standard Lagrange multipliers with global factorization. Middle: Bézier dual basis with global factorization. Right: Bézier dual basis with localized factorization. Top: original matrix. Bottom: small absolute values ( $\leq 10^{-14}$ ) be pruned. All stiffness matrices are formulated for the three-patch coupling in Figure 5 with 3<sup>rd</sup> order B-spline basis functions after 4 refinements. The number of non-zero entries is given by nz.

698 projection of constant function is below the round-off error. The results of  
 699 projecting Legendre polynomials up to 3<sup>rd</sup> order onto 3<sup>rd</sup> order Bézier dual  
 700 basis are demonstrated in Fig. 11. As can be seen, there are huge discrep-  
 701 ancies between the approximations and original functions for all Legendre  
 702 polynomials except constant. In other words, the  $L^2$  approximation of Bézier  
 703 dual basis is only of first-order, which might deteriorate the optimality of the  
 704 finite element approximation.

705 In the finite element context, the construction of dual basis that can  
 706 reproduce polynomial of degree  $p - 1$  is thoroughly studied in [70]. However,  
 707 the construction procedure is complicated and gets even worse for higher  
 708 inter-element continuity. Following this approach, a  $p - 1$  complete dual  
 709 basis function for a quadratic B-spline basis function was constructed in [21],

710 but its support is much larger than its B-spline counterpart. On the other  
 711 side, though the poor polynomial completeness, Bézier dual basis can be  
 712 constructed in a straightforward manner, without solving additional linear  
 713 system. Hence, in the rest examples, we will testify the performance of  $C^1$   
 714 dual mortaring and the influence of the Bézier dual basis on the optimality  
 715 of the finite element approximation.

716 *7.2. Biharmonic problem on a two-patch domain with homogeneous Dirichlet  
 717 Boundary*

718 We first solve a biharmonic problem  $\Delta^2 u = f$  on a square domain  $\Omega =$   
 719  $(0, 1) \times (0, 1)$ . The manufacrtued solution is given as

$$u(x, y) = \sin(3\pi x)^2 \sin(3\pi y)^2, \quad (82)$$

720 which satisfies the homogeneous Dirichlet boundary condition ( $u = \frac{\partial u}{\partial n} =$   
 721 0) and is visualized in Figure. 12. The domain  $\Omega$  is decomposed into two  
 722 patches, namely  $\Omega_1 = (0, 0.4) \times (0, 1)$  and  $\Omega_2 = (0.4, 1) \times (0, 1)$ , as shown in  
 723 Figure. 12a. The right-hand side function  $f$  can be obtained by applying the  
 724 biharmonic operator to  $u$ .

725 We conduct convergence studies for  $p = 2, 3, 4, 5$  in both  $L^2$  norm and  
 726  $H^2$  norm, as shown in Fig. 13. However, though the theoretical flaw of  
 727 Bézier dual basis, its performances in real problem are surprisingly well. As  
 728 can be seen, both global dual basis and Bézier dual basis obtain optimal  
 729 convergence rate in both norm measures for all polynomial degrees (The op-  
 730 timal convergence rate for  $p = 2$  in  $L^2$  norm is 2, which can be testified by  
 731 Aubin-Nitsche duality argument[10]). One conjecture can be made is that  
 732 for biharmonic problems, the coefficients of the best approximation error of  
 733 Lagrange multipliers are very small so that their contribution in the finite el-  
 734 ement approximation error can be ignored. Moreover, the accuracy of Bézier  
 735 dual basis are higher than that of global dual basis with the same refinement  
 736 level.

737 To study the performance of proposed methods in detail, we consider ex-  
 738 treme conditions e.g. distorted mesh (Figure. 12b), mismatched mesh (Fig-  
 739 ure. 12c) and mismatched degree ( $p_1 = p_2 + 1$ ), respectively. For the distorted  
 740 mesh, the proposed method with both global dual basis and Bézier dual ba-  
 741 sis perform similarly, the optimal convergence rates are reached for all cases.  
 742 Some superconvergence behavior are observed (e.g.  $p = 3$  for both global and  
 743 Bézier dual basis). This partially due to the geometrical locking existed in

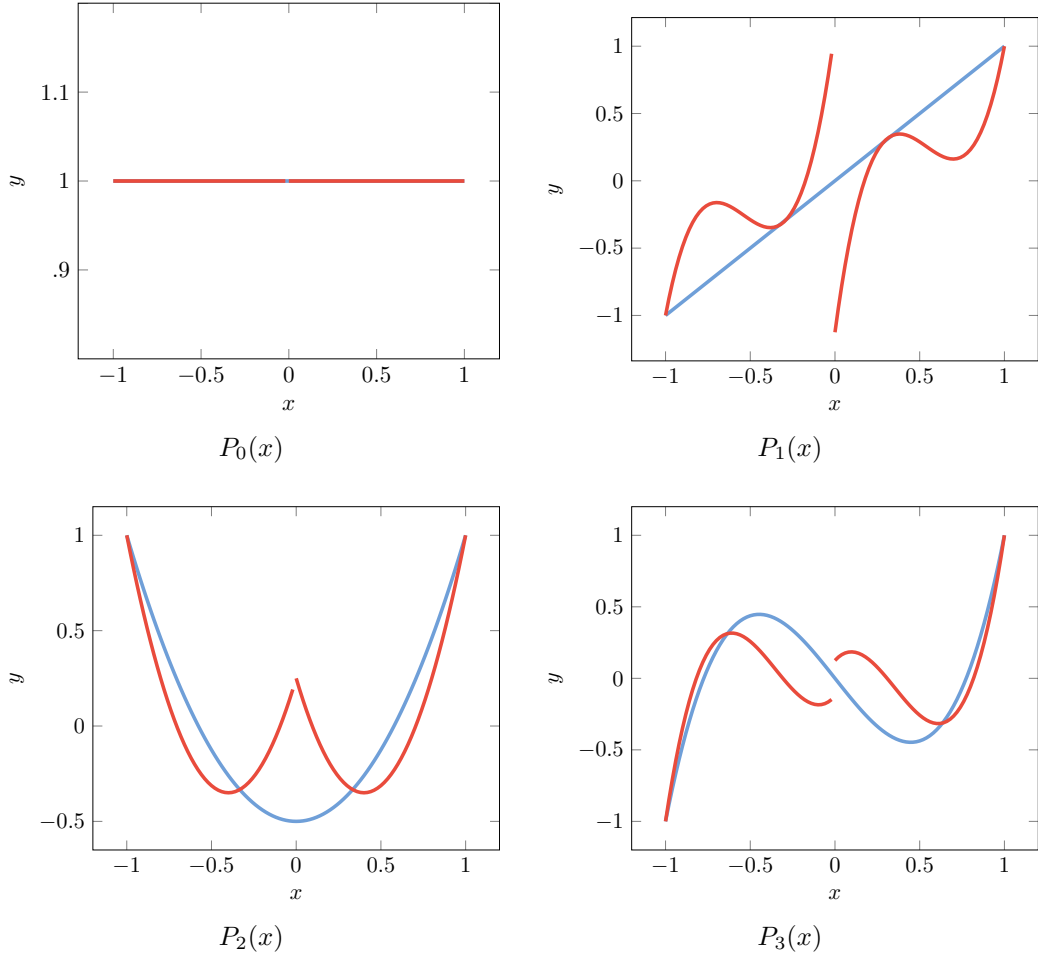


Figure 11: The Legendre polynomials (—) and their approximations (—) in  $3^{rd}$  order Bézier dual space composed of two elements. Bézier dual basis cannot duplicate all except the constant function.

744 deformed meshes. For the mismatched mesh, the convergence performance  
 745 of Bézier dual basis, though remains optimality, suffers a vertical lift of the  
 746 error curves, which indicates that the Bézier dual basis are more sensitive to  
 747 the mesh quality. However, for the finer mesh, the result obtained by 5<sup>th</sup> or-  
 748 der global dual basis become sub-optimal, we speculate this is caused by the  
 749 *inf-sup* instability in this specific circumstance. For the degree mismatched  
 750 case, as expected, the convergence rates are between  $p + 1$  and  $p + 2$  in  $L^2$   
 751 norm, and between  $p - 1$  and  $p$  in  $H^2$  norm for all tested cases.

752 Although a functional analysis of the contributions of the Lagrange mul-  
 753 tipliers' best approximation error in the finite element approximation error is  
 754 beyond the scope of this paper and postponed to future work, here we study  
 755 their influence in a numerical manner. The best approximation of  $u$  in the  
 756 discretized weak  $C^1$  space  $\mathcal{K}_b^h$  can be given as: find  $u \in \mathcal{K}_b^h$  such that

$$\langle v^h, u^h \rangle_{H^2} = \langle v^h, u \rangle_{H^2} \quad \forall v^h \in \mathcal{K}_b^h. \quad (83)$$

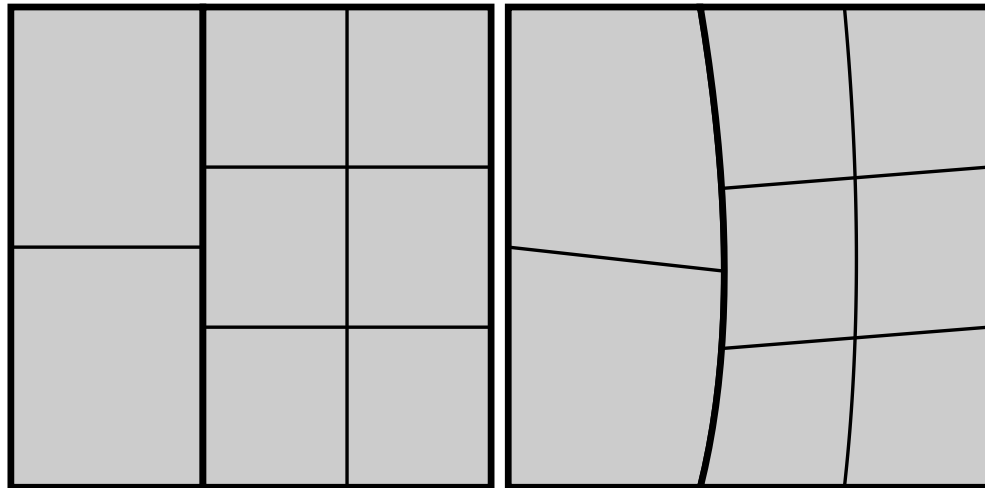
757 The best  $H^2$  approximation error for the proposed methods for all sce-  
 758 narios are shown in Fig. 17. As can be seen, the convergence plots of the best  
 759  $H^2$  approximation error are identical to that of the finite element approxi-  
 760 mation error in  $H^2$  norm. The best  $H^2$  approximation errors for all cases are  
 761 no more than 1% smaller than that of the finite element counterparts, which  
 762 confirms our speculation that the contribution of the Lagrange multipliers'  
 763 best approximation errors are negligible for tested problems. In addition, the  
 764 best approximation error for the  $p = 5$  global dual basis in the mismatched  
 765 non-conforming mesh test case also suffers rate decay, which confirms that  
 766 the main cause of the rate decay is due to the *inf – sup* instability.

767 *7.3. Biharmonic problem on a three-patch domain with homogeneous Dirich-  
 768 let Boundary*

769 **8. Schedule**

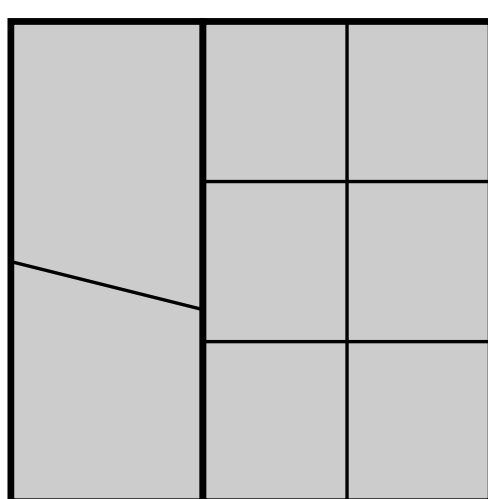
770 Although there are various aspects in weak  $C^1/G^1$  coupling deserve a  
 771 thorough study, our main focus in this stage is to extend our finding in an ab-  
 772 stract problem (biharmonic problem) to practical problems (e.g. Kirchhoff-  
 773 Love shell). Compared to the planar biharmonic problem, Kirchhoff-Love  
 774 shell is a more challenging problem, as the computational domain is in  $\mathbb{R}^3$   
 775 and the constraint is not isotropically applied in each direction. Hence, a  
 776 more generalized constraint is needed to compromise geometries with kinks.  
 777 And validations are needed for two-patch and multi-patch Kirchhoff-Love

778 shells. Meanwhile, although we have implemented two algorithms to solve  
779 multi-patch biharmonic problems, the boundary modification method does  
780 not deliver ideal results while an additional factorization is needed for ex-  
781 plicitly solving the null space. We will still make efforts in finding a feasi-  
782 ble boundary modification for multi-patch coupling. A detailed time line is  
783 shown in Table. 2.

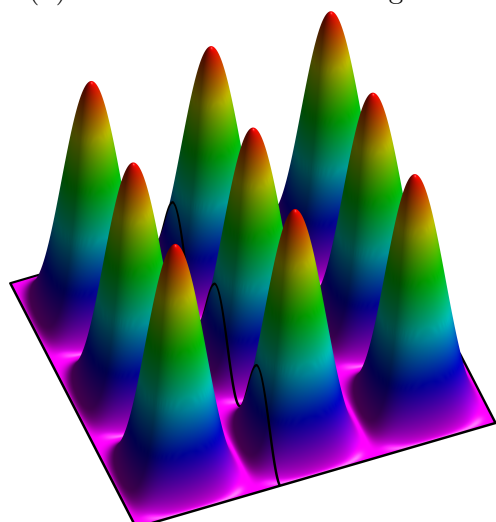


(a) Simple non-conforming mesh

(b) Distorted non-conforming mesh



(c) mismatched non-conforming mesh



(d) Reference solution

Figure 12: The discretizations of computational domain  $\Omega$  and the manufactured solution with the property  $u = \frac{\partial u}{\partial \mathbf{n}} = 0$  on  $\partial\Omega$ , which are used in Section 7.2.

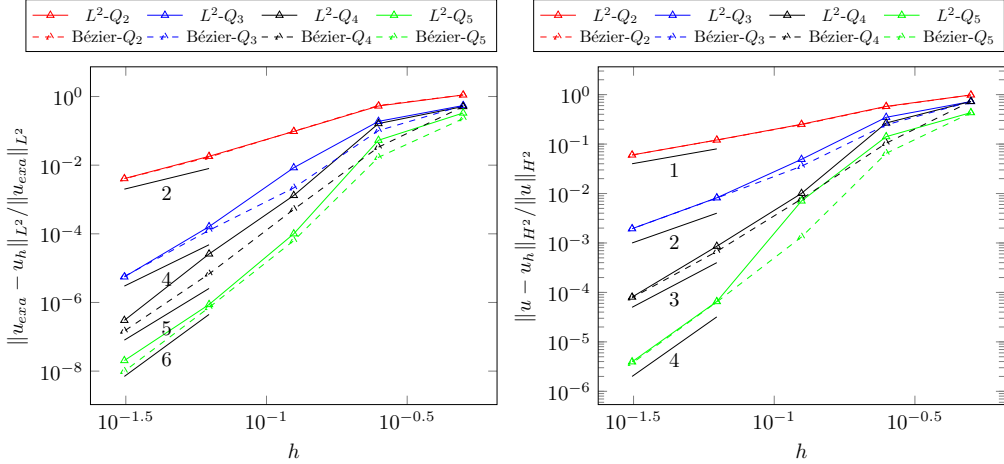


Figure 13: Convergence plot for simple non-conforming patch coupling in 7.2. Left: error measured in  $L^2$  norm. Right: error measured in  $H^2$  norm.

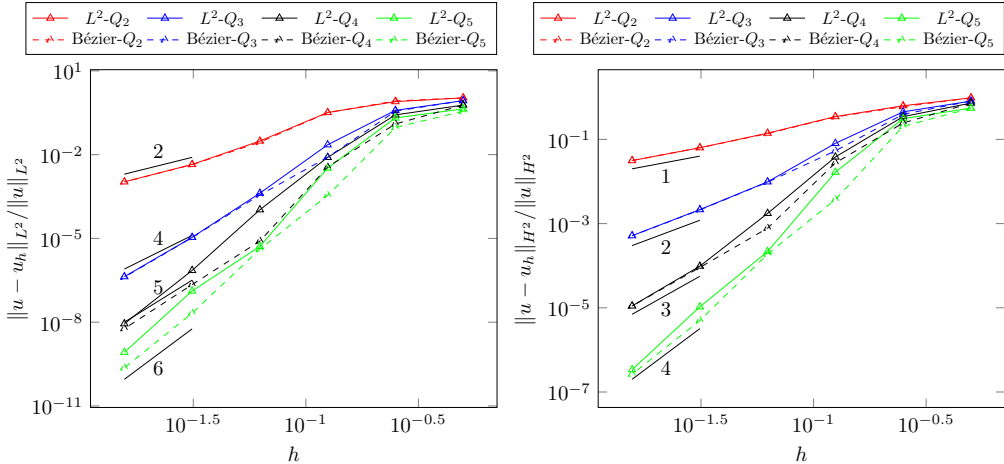


Figure 14: Convergence plot for distorted non-conforming patch coupling in 7.2. Left: error measured in  $L^2$  norm. Right: error measured in  $H^2$  norm.

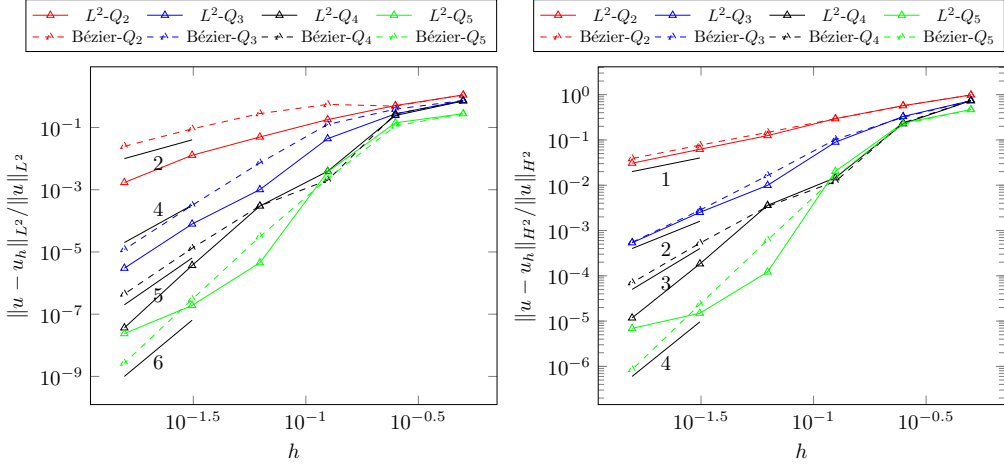


Figure 15: Convergence plot for mesh mismatched non-conforming patch coupling in 7.2. Left: error measured in  $L^2$  norm. Right: error measured in  $H^2$  norm.

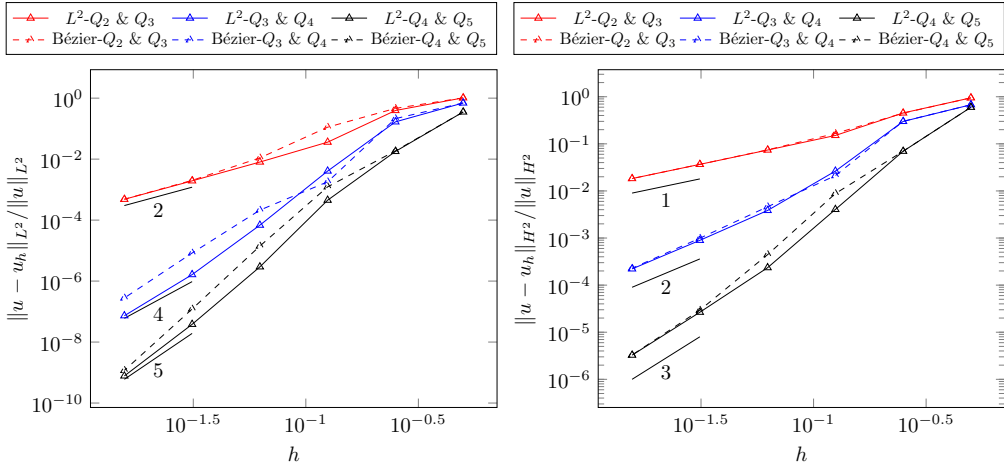


Figure 16: Convergence plot for degree mismatched non-conforming patch coupling in 7.2. Left: error measured in  $L^2$  norm. Right: error measured in  $H^2$  norm.

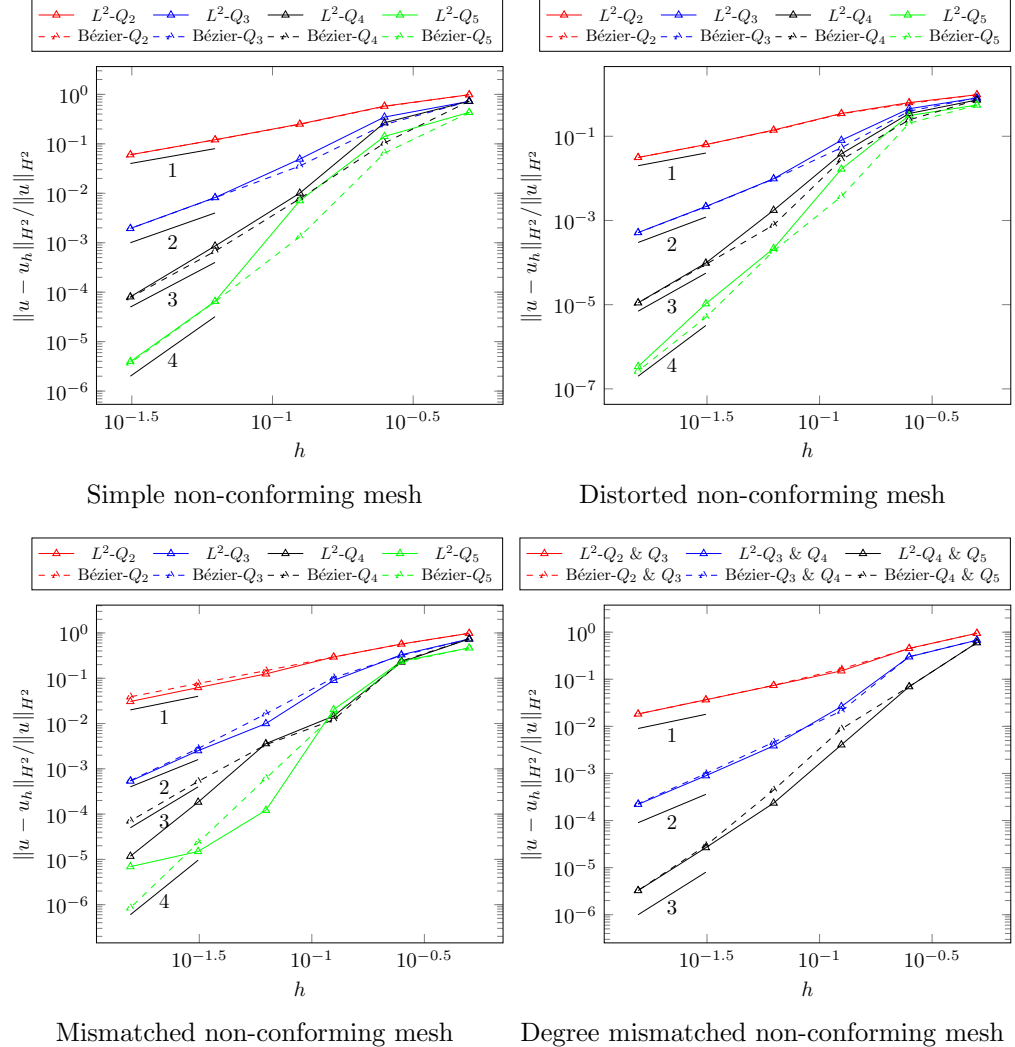
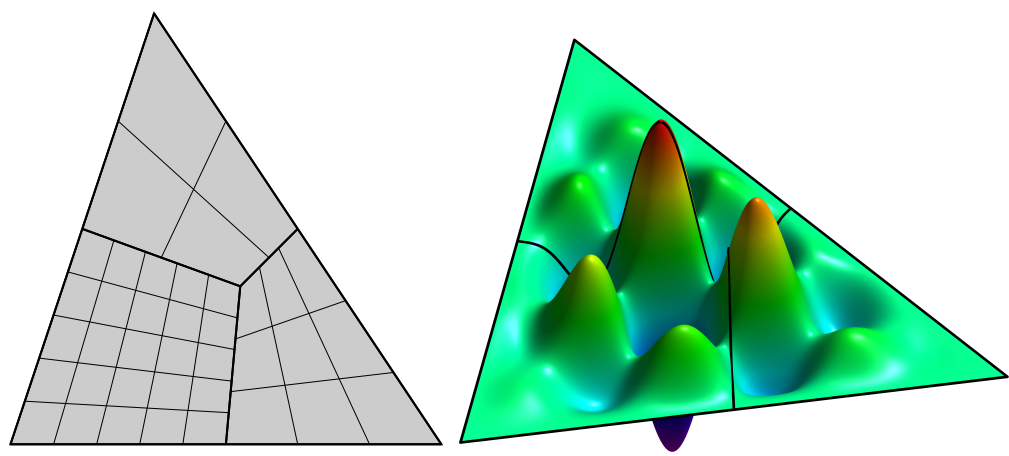


Figure 17: Convergence plot of the best  $H^2$  approximation error for non-conforming patch coupling in 7.2.

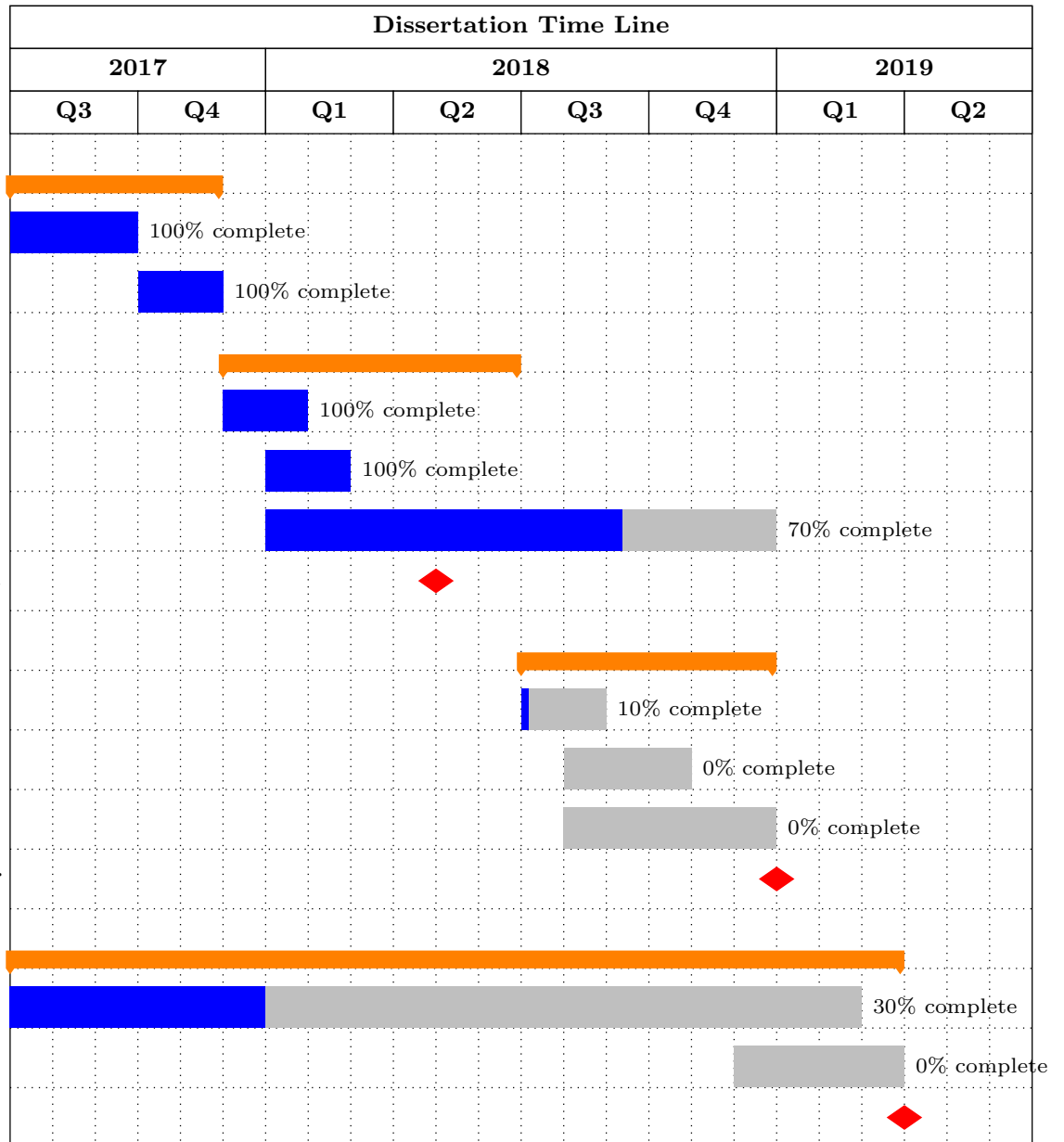


(a) Non-conforming mesh

(b) Reference solution

Figure 18: Convergence plot of the best  $H^2$  approximation error for non-conforming patch coupling in 7.2.

Table 2: A schedule of tasks and stages of my research towards the final dissertation.



- 784 [1] Andreas Apostolatos, Michael Breitenberger, Roland Wüchner, and Kai-  
 785 Uwe Bletzinger. Domain decomposition methods and kirchhoff-love shell  
 786 multipatch coupling in isogeometric analysis. In *Isogeometric Analysis*  
 787 and Applications 2014, pages 73–101. Springer, 2015.
- 788 [2] Andreas Apostolatos, Robert Schmidt, Roland Wüchner, and Kai-Uwe  
 789 Bletzinger. A Nitsche-type formulation and comparison of the most  
 790 common domain decomposition methods in isogeometric analysis. *International*  
 791 *Journal for Numerical Methods in Engineering*, 97(7):473–504,  
 792 February 2014.
- 793 [3] Helio JC Barbosa and Thomas JR Hughes. The finite element method  
 794 with lagrange multipliers on the boundary: circumventing the babuška-  
 795 brezzi condition. *Computer Methods in Applied Mechanics and Engi-*  
 796 *neering*, 85(1):109–128, 1991.
- 797 [4] Y. Bazilevs, V. M. Calo, J. A. Cottrell, J. A. Evans, T. J. R. Hughes,  
 798 S. Lipton, M. A. Scott, and T. W. Sederberg. Isogeometric analysis using  
 799 T-splines. *Computer Methods in Applied Mechanics and Engineering*,  
 800 199(5–8):229–263, January 2010.
- 801 [5] Yuri Bazilevs, L Beirao da Veiga, J Austin Cottrell, Thomas JR Hughes,  
 802 and Giancarlo Sangalli. Isogeometric analysis: approximation, stabil-  
 803 ity and error estimates for h-refined meshes. *Mathematical Models and*  
 804 *Methods in Applied Sciences*, 16(07):1031–1090, 2006.
- 805 [6] Roland Becker, Peter Hansbo, and Rolf Stenberg. A finite ele-  
 806 ment method for domain decomposition with non-matching grids.  
 807 *ESAIM: Mathematical Modelling and Numerical Analysis - Modélisation*  
 808 *Mathématique et Analyse Numérique*, 37(2):209–225, 2003.
- 809 [7] F. B. Belgacem, P. Hild, and P. Laborde. The mortar finite element  
 810 method for contact problems. *Mathematical and Computer Modelling*,  
 811 28(4):263–271, August 1998.
- 812 [8] Faker Ben Belgacem. The Mortar finite element method with Lagrange  
 813 multipliers. *Numerische Mathematik*, 84(2):173–197, December 1999.
- 814 [9] FAKER BEN BELGACEM, Patrick Hild, and Patrick Laborde. Ex-  
 815 tension of the mortar finite element method to a variational inequality

- 816 modeling unilateral contact. *Mathematical Models and Methods in Applied Sciences*, 9(02):287–303, 1999.
- 817
- 818 [10] Zakaria Belhachmi and Christine Bernardi. Resolution of fourth-order  
819 problems by the mortar element method. *Computer Methods in Applied Mechanics and Engineering*, 116(1):53–58, January 1994.
- 820
- 821 [11] Michele Benzi and Andrew J. Wathen. Some Preconditioning Techniques for Saddle Point Problems. In Wilhelmus H. A. Schilders, Henk A. van der Vorst, and Joost Rommes, editors, *Model Order Reduction: Theory, Research Aspects and Applications*, number 13 in Mathematics in Industry, pages 195–211. Springer Berlin Heidelberg, 2008. DOI: 10.1007/978-3-540-78841-6\_10.
- 822
- 823
- 824
- 825
- 826
- 827 [12] Michel Bercovier and Tanya Matskewich. Smooth Bezier Surfaces over Arbitrary Quadrilateral Meshes. *arXiv:1412.1125 [math]*, December 2014. arXiv: 1412.1125.
- 828
- 829
- 830 [13] C. Bernardi, Y. Maday, and A. T. Patera. Domain Decomposition by the Mortar Element Method. In Hans G. Kaper, Marc Garbey, and Gail W. Pieper, editors, *Asymptotic and Numerical Methods for Partial Differential Equations with Critical Parameters*, pages 269–286. Springer Netherlands, Dordrecht, 1993. DOI: 10.1007/978-94-011-1810-1\_17.
- 831
- 832
- 833
- 834
- 835 [14] Christine Bernardi, Yvon Maday, and Francesca Rapetti. Basics and some applications of the mortar element method. *GAMM-Mitteilungen*, 28(2):97–123, November 2005.
- 836
- 837
- 838 [15] Daniele Boffi, Franco Brezzi, and Michel Fortin. *Mixed Finite Element Methods and Applications*. Springer Series in Computational Mathematics. Springer-Verlag.
- 839
- 840
- 841 [16] Michael J Borden, Thomas JR Hughes, Chad M Landis, and Clemens V Verhoosel. A higher-order phase-field model for brittle fracture: Formulation and analysis within the isogeometric analysis framework. *Computer Methods in Applied Mechanics and Engineering*, 273:100–118, 2014.
- 842
- 843
- 844
- 845
- 846 [17] Michael J Borden, Clemens V Verhoosel, Michael A Scott, Thomas JR Hughes, and Chad M Landis. A phase-field description of dynamic brit-
- 847

- 848       tle fracture. *Computer Methods in Applied Mechanics and Engineering*,  
 849       217:77–95, 2012.
- 850 [18] P. B. Bornemann and F. Cirak. A subdivision-based implementation of  
 851       the hierarchical b-spline finite element method. *Computer Methods in*  
 852       *Applied Mechanics and Engineering*, 253:584–598, January 2013.
- 853 [19] Robin Bouclier, Jean-Charles Passieux, and Michel Salaün. Develop-  
 854       ment of a new, more regular, mortar method for the coupling of NURBS  
 855       subdomains within a NURBS patch: Application to a non-intrusive local  
 856       enrichment of NURBS patches. *Computer Methods in Applied Mechan-*  
 857       *ics and Engineering*, 316:123–150, April 2017.
- 858 [20] Susanne Brenner and Ridgway Scott. *The Mathematical Theory of Fi-*  
 859       *nite Element Methods*. Springer Science & Business Media, December  
 860       2007. Google-Books-ID: ci4c\_R0WKYYC.
- 861 [21] Ericka Brivadis, Annalisa Buffa, Barbara Wohlmuth, and Linus Wun-  
 862       derlich. Isogeometric mortar methods. *Computer Methods in Applied*  
 863       *Mechanics and Engineering*, 284:292–319, February 2015.
- 864 [22] A. Buffa, D. Cho, and G. Sangalli. Linear independence of the T-spline  
 865       blending functions associated with some particular T-meshes. *Computer*  
 866       *Methods in Applied Mechanics and Engineering*, 199(23–24):1437–1445,  
 867       April 2010.
- 868 [23] E. Catmull and J. Clark. Recursively generated B-spline surfaces on  
 869       arbitrary topological meshes. *Computer-Aided Design*, 10(6):350–355,  
 870       November 1978.
- 871 [24] Franz Chouly, Patrick Hild, and Yves Renard. Symmetric and non-  
 872       symmetric variants of Nitsche’s method for contact problems in elasticity:  
 873       theory and numerical experiments. *Mathematics of Computation*,  
 874       84(293):1089–1112, 2015.
- 875 [25] Annabelle Collin, Giancarlo Sangalli, and Thomas Takacs. Analysis-  
 876       suitable G1 multi-patch parametrizations for C1 isogeometric spaces.  
 877       *Computer Aided Geometric Design*, 47:93–113, October 2016.
- 878 [26] Laurens Coox, Onur Atak, Dirk Vandepitte, and Wim Desmet. An isoge-  
 879       ometric indirect boundary element method for solving acoustic problems

- 880       in open-boundary domains. *Computer Methods in Applied Mechanics*  
 881       and *Engineering*, 316:186–208, April 2017.
- 882 [27] Laurens Coox, Francesco Greco, Onur Atak, Dirk Vandepitte, and Wim  
 883       Desmet. A robust patch coupling method for NURBS-based isogeometric  
 884       analysis of non-conforming multipatch surfaces. *Computer Methods*  
 885       in *Applied Mechanics and Engineering*, 316:235–260, April 2017.
- 886 [28] Laurens Coox, Florian Maurin, Francesco Greco, Elke Deckers, Dirk  
 887       Vandepitte, and Wim Desmet. A flexible approach for coupling nurbs  
 888       patches in rotationless isogeometric analysis of kirchhoff–love shells.  
 889       *Computer Methods in Applied Mechanics and Engineering*, 325:505–531,  
 890       2017.
- 891 [29] L Beirao Da Veiga, Annalisa Buffa, Judith Rivas, and Giancarlo Sangalli.  
 892       Some estimates for h–p–k-refinement in isogeometric analysis. *Nu-  
 893       merische Mathematik*, 118(2):271–305, 2011.
- 894 [30] L Beirao Da Veiga, Annalisa Buffa, Giancarlo Sangalli, and Rafael  
 895       Vázquez. Mathematical analysis of variational isogeometric methods.  
 896       *Acta Numerica*, 23:157–287, 2014.
- 897 [31] D. Doo and M. Sabin. Behaviour of recursive division surfaces near ex-  
 898       traordinary points. *Computer-Aided Design*, 10(6):356–360, November  
 899       1978.
- 900 [32] W Dornisch, J Stöckler, and R Müller. Dual and approximate dual  
 901       basis functions for b-splines and nurbs—comparison and application for  
 902       an efficient coupling of patches with the isogeometric mortar method.  
 903       *Computer Methods in Applied Mechanics and Engineering*, 316:449–496,  
 904       2017.
- 905 [33] W. Dornisch, J. Stöckler, and R. Müller. Dual and approximate dual  
 906       basis functions for B-splines and NURBS – Comparison and application  
 907       for an efficient coupling of patches with the isogeometric mortar method.  
 908       *Computer Methods in Applied Mechanics and Engineering*, 316:449–496,  
 909       April 2017.
- 910 [34] W. Dornisch, G. Vitucci, and S. Klinkel. The weak substitution method  
 911       – an application of the mortar method for patch coupling in NURBS-

- 912 based isogeometric analysis. *International Journal for Numerical Methods in Engineering*, 103(3):205–234, July 2015.
- 913
- 914 [35] Wolfgang Dornisch and Sven Klinkel. Boundary conditions and multi-  
915 patch connections in isogeometric analysis. *PAMM*, 11(1):207–208, 2011.
- 916 [36] Wolfgang Dornisch and Ralf Müller. Patch coupling with the isogeomet-  
917 ric dual mortar approach. *PAMM*, 16(1):193–194, October 2016.
- 918 [37] Michael R. Dörfel, Bert Jüttler, and Bernd Simeon. Adaptive isogeomet-  
919 ric analysis by local h-refinement with T-splines. *Computer Methods in  
920 Applied Mechanics and Engineering*, 199(5–8):264–275, January 2010.
- 921 [38] Anand Embar, John Dolbow, and Isaac Harari. Imposing Dirichlet  
922 boundary conditions with Nitsche’s method and spline-based finite el-  
923 ements. *International Journal for Numerical Methods in Engineering*,  
924 83(7):877–898, August 2010.
- 925 [39] Charbel Farhat, Po-Shu Chen, and Jan Mandel. A scalable Lagrange  
926 multiplier based domain decomposition method for time-dependent  
927 problems. *International Journal for Numerical Methods in Engineering*,  
928 38(22):3831–3853, November 1995.
- 929 [40] David R. Forsey and Richard H. Bartels. Hierarchical B-spline Re-  
930 finement. In *Proceedings of the 15th Annual Conference on Computer  
931 Graphics and Interactive Techniques*, SIGGRAPH ’88, pages 205–212,  
932 New York, NY, USA, 1988. ACM.
- 933 [41] Carlotta Giannelli, Bert Jüttler, and Hendrik Speleers. THB-splines:  
934 The truncated basis for hierarchical splines. *Computer Aided Geometric  
935 Design*, 29(7):485–498, October 2012.
- 936 [42] Héctor Gómez, Victor M Calo, Yuri Bazilevs, and Thomas JR Hughes.  
937 Isogeometric analysis of the cahn–hilliard phase-field model. *Computer  
938 methods in applied mechanics and engineering*, 197(49–50):4333–4352,  
939 2008.
- 940 [43] David Groisser and Jörg Peters. Matched -constructions always yield  
941 -continuous isogeometric elements. *Computer Aided Geometric Design*,  
942 34:67–72, March 2015.

- 943 [44] Yujie Guo and Martin Ruess. Nitsche's method for a coupling of isogeometric thin shells and blended shell structures. *Computer Methods in Applied Mechanics and Engineering*, 284:881–905, February 2015.
- 944
- 945
- 946 [45] Peter Hansbo. Nitsche's method for interface problems in computational mechanics. *GAMM-Mitteilungen*, 28(2):183–206, November 2005.
- 947
- 948 [46] Peter Hansbo, Carlo Lovadina, Ilaria Perugia, and Giancarlo Sangalli. A lagrange multiplier method for the finite element solution of elliptic interface problems using non-matching meshes. *Numerische Mathematik*, 100(1):91–115, 2005.
- 949
- 950
- 951
- 952 [47] Christian Hesch and Peter Betsch. Isogeometric analysis and domain decomposition methods. *Computer Methods in Applied Mechanics and Engineering*, 213–216:104–112, March 2012.
- 953
- 954
- 955 [48] Stefan Hüeber and Barbara I Wohlmuth. A primal–dual active set strategy for non-linear multibody contact problems. *Computer Methods in Applied Mechanics and Engineering*, 194(27–29):3147–3166, 2005.
- 956
- 957
- 958 [49] T.J.R. Hughes, J.A. Cottrell, and Y. Bazilevs. Isogeometric analysis: Cad, finite elements, nurbs, exact geometry and mesh refinement. *Computer Methods in Applied Mechanics and Engineering*, 194(39):4135 – 4195, 2005.
- 959
- 960
- 961
- 962 [50] Mika Juntunen. On the connection between the stabilized lagrange multiplier and nitsche's methods. *Numerische Mathematik*, 131(3):453–471, 2015.
- 963
- 964
- 965 [51] Bert Jüttler, Angelos Mantzaflaris, Ricardo Perl, and Martin Rumpf. On numerical integration in isogeometric subdivision methods for PDEs on surfaces. *Computer Methods in Applied Mechanics and Engineering*, 302:131–146, April 2016.
- 966
- 967
- 968
- 969 [52] Hongmei Kang, Xin Li, Falai Chen, and Jiansong Deng. Truncated Hierarchical Loop Subdivision Surfaces and application in isogeometric analysis. *Computers & Mathematics with Applications*, 72(8):2041–2055, October 2016.
- 970
- 971
- 972
- 973 [53] Mario Kapl, Florian Buchegger, Michel Bercovier, and Bert Jüttler. Iso-geometric analysis with geometrically continuous functions on planar
- 974

- 975        multi-patch geometries. *Computer Methods in Applied Mechanics and*  
 976        *Engineering*, 316:209–234, April 2017.
- 977 [54] Mario Kapl and Vito Vitrih. Space of -smooth geometrically continuous  
 978        isogeometric functions on planar multi-patch geometries: Dimension and  
 979        numerical experiments. *Computers & Mathematics with Applications*.
- 980 [55] Mario Kapl and Vito Vitrih. Space of -smooth geometrically continuous  
 981        isogeometric functions on two-patch geometries. *Computers & Mathe-*  
 982        *matics with Applications*, 73(1):37–59, January 2017.
- 983 [56] Mario Kapl, Vito Vitrih, Bert Jüttler, and Katharina Birner. Isoge-  
 984        ometric analysis with geometrically continuous functions on two-patch  
 985        geometries. *Computers & Mathematics with Applications*, 70(7):1518–  
 986        1538, October 2015.
- 987 [57] J Kiendl, Y Bazilevs, M-C Hsu, R Wüchner, and K-U Bletzinger. The  
 988        bending strip method for isogeometric analysis of kirchhoff–love shell  
 989        structures comprised of multiple patches. *Computer Methods in Applied*  
 990        *Mechanics and Engineering*, 199(37-40):2403–2416, 2010.
- 991 [58] J Kiendl, K-U Bletzinger, J Linhard, and R Wüchner. Isogeometric shell  
 992        analysis with kirchhoff–love elements. *Computer Methods in Applied*  
 993        *Mechanics and Engineering*, 198(49-52):3902–3914, 2009.
- 994 [59] Josef Kiendl, Ming-Chen Hsu, Michael CH Wu, and Alessandro Reali.  
 995        Isogeometric kirchhoff–love shell formulations for general hyperelastic  
 996        materials. *Computer Methods in Applied Mechanics and Engineering*,  
 997        291:280–303, 2015.
- 998 [60] Bishnu Prasad Lamichhane. Higher order mortar finite elements with  
 999        dual lagrange multiplier spaces and applications.
- 1000 [61] Bishnu Prasad Lamichhane and Barbara I Wohlmuth. Higher order  
 1001        dual lagrange multiplier spaces for mortar finite element discretizations.  
 1002        *Calcolo*, 39(4):219–237, 2002.
- 1003 [62] Xin Li and M. A. Scott. Analysis-suitable T-splines: Characterization,  
 1004        refineability, and approximation. *Mathematical Models and Methods in*  
 1005        *Applied Sciences*, 24(06):1141–1164, October 2013.

- 1006 [63] Xin Li, Jianmin Zheng, Thomas W. Sederberg, Thomas J. R. Hughes,  
 1007 and Michael A. Scott. On linear independence of T-spline blending func-  
 1008 tions. *Computer Aided Geometric Design*, 29(1):63–76, January 2012.
- 1009 [64] Charles Teorell Loop and Charles Loop. Smooth Subdivision Surfaces  
 1010 Based on Triangles. January 1987.
- 1011 [65] Leszek Marcinkowski. Mortar methods for some second and fourth order  
 1012 elliptic equations. *Distinguished Ph. D. Thesis*, 1999.
- 1013 [66] Stephen E Moore. Discontinuous galerkin isogeometric analysis for the  
 1014 biharmonic equation. *arXiv preprint arXiv:1703.02726*, 2017.
- 1015 [67] Thien Nguyen, Keçstutis Karčiauskas, and Jörg Peters. A Comparative  
 1016 Study of Several Classical, Discrete Differential and Isogeometric Meth-  
 1017 ods for Solving Poisson’s Equation on the Disk. *Axioms*, 3(2):280–299,  
 1018 June 2014.
- 1019 [68] Vinh Phu Nguyen, Pierre Kerfriden, Marco Brino, Stéphane P. A. Bor-  
 1020 das, and Elvio Bonisoli. Nitsche’s method for two and three dimensional  
 1021 NURBS patch coupling. *Computational Mechanics*, 53(6):1163–1182,  
 1022 June 2014.
- 1023 [69] J. Nitsche. Über ein Variationsprinzip zur Lösung von Dirichlet-  
 1024 Problemen bei Verwendung von Teilräumen, die keinen Randbedingun-  
 1025 gen unterworfen sind. *Abhandlungen aus dem Mathematischen Seminar  
 1026 der Universität Hamburg*, 36(1):9–15, July 1971.
- 1027 [70] Peter Oswald and Barbara Wohlmuth. On polynomial reproduction of  
 1028 dual fe bases. In *Thirteenth international conference on domain decom-  
 1029 position methods*, pages 85–96, 2001.
- 1030 [71] Qing Pan, Guoliang Xu, Gang Xu, and Yongjie Zhang. Isogeometric  
 1031 analysis based on extended Loop’s subdivision. *Journal of Compu-  
 1032 tational Physics*, 299:731–746, October 2015.
- 1033 [72] Jörg Peters. Joining smooth patches around a vertex to form a C<sub>k</sub>  
 1034 surface. *Computer Aided Geometric Design*, 9(5):387–411, November  
 1035 1992.

- 1036 [73] Jörg Peters. Chapter 8 - Geometric Continuity. In *Handbook of Computer Aided Geometric Design*, pages 193–227. North-Holland, Amsterdam, 2002. DOI: 10.1016/B978-044451104-1/50009-5.
- 1037  
1038
- 1039 [74] Alexander Popp, Michael W Gee, and Wolfgang A Wall. A finite de-
- 1040 formation mortar contact formulation using a primal–dual active set
- 1041 strategy. *International Journal for Numerical Methods in Engineering*,
- 1042 79(11):1354–1391, 2009.
- 1043 [75] Beatrice Riviere. *Discontinuous Galerkin methods for solving elliptic*
- 1044 *and parabolic equations: theory and implementation*. SIAM, 2008.
- 1045 [76] M. A. Scott, X. Li, T. W. Sederberg, and T. J. R. Hughes. Local
- 1046 refinement of analysis-suitable T-splines. *Computer Methods in Applied*
- 1047 *Mechanics and Engineering*, 213–216:206–222, March 2012.
- 1048 [77] M. A. Scott, R. N. Simpson, J. A. Evans, S. Lipton, S. P. A. Bordas,
- 1049 T. J. R. Hughes, and T. W. Sederberg. Isogeometric boundary element
- 1050 analysis using unstructured T-splines. *Computer Methods in Applied*
- 1051 *Mechanics and Engineering*, 254:197–221, February 2013.
- 1052 [78] Michael A. Scott, Michael J. Borden, Clemens V. Verhoosel, Thomas W.
- 1053 Sederberg, and Thomas J. R. Hughes. Isogeometric finite element data
- 1054 structures based on Bézier extraction of T-splines. *International Journal*
- 1055 *for Numerical Methods in Engineering*, 88(2):126–156, October 2011.
- 1056 [79] Thomas W. Sederberg, Jianmin Zheng, Almaz Bakenov, and Ahmad
- 1057 Nasri. T-splines and T-NURCCs. In *ACM SIGGRAPH 2003 Papers*,
- 1058 SIGGRAPH ’03, pages 477–484, New York, NY, USA, 2003. ACM.
- 1059 [80] Alexander Seitz, Philipp Farah, Johannes Kremheller, Barbara I.
- 1060 Wohlmuth, Wolfgang A. Wall, and Alexander Popp. Isogeometric dual
- 1061 mortar methods for computational contact mechanics. *Computer Meth-*
- 1062 *ods in Applied Mechanics and Engineering*, 301:259–280, April 2016.
- 1063 [81] Juan C Simo, Peter Wriggers, and Robert L Taylor. A perturbed la-
- 1064 grangian formulation for the finite element solution of contact problems.
- 1065 *Computer methods in applied mechanics and engineering*, 50(2):163–180,
- 1066 1985.

- 1067 [82] Rolf Stenberg. On some techniques for approximating boundary con-  
 1068     ditions in the finite element method. *Journal of Computational and*  
 1069     *applied Mathematics*, 63(1-3):139–148, 1995.
- 1070 [83] Gilbert Strang and George Fix. *An Analysis of the Finite Element*  
 1071     *Method*. Wellesley-Cambridge Press, May 2008. Google-Books-ID:  
 1072      K5MAOwAACAAJ.
- 1073 [84] Radek Tezaur. *Analysis of Lagrange multiplier based domain decompo-*  
 1074     *sition*. PhD thesis, University of Colorado at Denver, 1998.
- 1075 [85] Derek C Thomas, Michael A Scott, John A Evans, Kevin Tew, and  
 1076      Emily J Evans. Bézier projection: a unified approach for local pro-  
 1077      jection and quadrature-free refinement and coarsening of nurbs and t-  
 1078      splines with particular application to isogeometric design and analysis.  
 1079      *Computer Methods in Applied Mechanics and Engineering*, 284:55–105,  
 1080      2015.
- 1081 [86] Manuel Tur, Jose Albelda, Jose Manuel Navarro-Jimenez, and Juan Jose  
 1082      Rodenas. A modified perturbed lagrangian formulation for contact prob-  
 1083      lems. *Computational Mechanics*, 55(4):737–754, 2015.
- 1084 [87] A. V. Vuong, C. Giannelli, B. Jüttler, and B. Simeon. A hierarchical ap-  
 1085      proach to adaptive local refinement in isogeometric analysis. *Computer*  
 1086      *Methods in Applied Mechanics and Engineering*, 200(49–52):3554–3567,  
 1087      December 2011.
- 1088 [88] Xiaodong Wei, Yongjie Zhang, Thomas J. R. Hughes, and Michael A.  
 1089      Scott. Truncated hierarchical Catmull–Clark subdivision with local re-  
 1090      finement. *Computer Methods in Applied Mechanics and Engineering*,  
 1091      291:1–20, July 2015.
- 1092 [89] B. Wohlmuth. A Mortar Finite Element Method Using Dual Spaces  
 1093      for the Lagrange Multiplier. *SIAM Journal on Numerical Analysis*,  
 1094      38(3):989–1012, January 2000.
- 1095 [90] Barbara I Wohlmuth. A comparison of dual lagrange multiplier spaces  
 1096      for mortar finite element discretizations. *ESAIM: Mathematical Mod-*  
 1097      *elling and Numerical Analysis*, 36(6):995–1012, 2002.

- 1098 [91] Xin Li. Some Properties for Analysis-Suitable T-Splines. *Journal of*  
1099 *Computational Mathematics*, 33(4):428–442, July 2015.
- 1100 [92] Olgierd Cecil Zienkiewicz, Robert Leroy Taylor, Olgierd Cecil  
1101 Zienkiewicz, and Robert Lee Taylor. *The finite element method*, vol-  
1102 ume 3. McGraw-hill London, 1977.